Oceanologia, 66 (4)/2024, 66403

https://doi.org/10.5697/EZNP4044

Variability and relationships between particle sizes, composition and optical properties of suspended particulate matter in the coastal waters of western Spitsbergen, assessed through measurements of size-fractionated seawater samples

Sławomir B. Woźniak*, Dagmara Litwicka, Joanna Stoń-Egiert

Abstract
Measurements of inherent optical properties (IOPs) and characteristics of concentration and composition of suspended particles were made on original and size-fractionated surface water samples from Arctic fjords and coastal waters of western Spitsbergen in the Svalbard archipelago, in the summer months of 2021 and 2022. Optical measurements included the spectral scattering coefficient of particles, and spectral absorption coefficients of particles as well as depigmented (non-algal) particles and phytoplankton. Assemblages of suspended particles were characterised by measuring the mass concentrations of suspended particulate matter (SPM), particulate organic matter (POM), particulate inorganic matter (PIM), and phytoplankton pigments including chlorophyll *a* (Chl*a*). All measurements were performed on original (unfiltered) seawater and on size-fractionated samples obtained by filtration using a combination of nylon meshes and membrane filters. This allowed us to determine the contribution of the fractions of very small (VS), small (S) and combined medium and large particles (ML) to the total SPM and Chl*a*, as well as to the total scattering and absorption coefficients. The obtained results: (i) indirectly indicate a clear variability in particle size distributions occurring in the studied marine environment (e.g., the contribution of ML size fraction to SPM (the ratio SPM_{ML}/SPM) varied between 0.10 and 0.52); (ii) indicate noticeable differences in composition between size fractions (e.g., the POM/SPM ratio was on average 0.21 for the S fraction, and 0.34 and 0.32 for the VS and ML fractions, respectively); (iii) in most cases indicate that the fraction S had the largest contribution to all analysed spectral optical coefficients, followed by the VS and ML fractions (the average contributions of the S fraction to scattering coefficient of particles and absorption coefficient of particles or depigmented (non-algal) particles were above 0.6 in the entire analysed spectral ranges); (iv) allowed for the identification of statistical relationships between selected characteristics describing changes in particle size and variability of particle IOPs (e.g., we observed statistical relations between SPM_{ML}/SPM and the spectral slope of scattering coefficient by particles, as well as SPM-specific coefficients of scattering by particles).

Keywords
Inherent optical properties (spectral scattering coefficient of particles, spectral absorption coefficients of particles, depigmented (non-algal) particles and phytoplankton); Composition of suspended particulate matter (mass concentrations of particulate organic matter, particulate inorganic matter, chlorophyll *a*); Seawater samples fractionated by particle size; Contributions of size fractions of suspended matter to particle concentration metrics and optical coefficients; Relations between metrics of size, composition and optical coefficients; Arctic coastal waters

Institute of Oceanology of the Polish Academy of Sciences, Powstańców Warszawy 55, 81–712 Sopot, Poland
***Correspondence**: woznjr@iopan.pl (S.B. Woźniak)

Received: 12 April 2024; **revised**: 10 July 2024; **accepted**: 5 September 2024

1. Introduction

The variability of the inherent optical properties (IOPs) of seawater is driven primarily by the changing concentration of various particles suspended in the water. But apart from the influence of particle concentration itself, it is also essential to determine what type of particles occur in given waters, what material they consist of, what their size distribution, and what their shape or internal structure is (see, e.g., Jonasz and Fournier, 2007; B. Woźniak and Dera, 2007; Mobley, 2022). Seawater may generally contain particles of very different origins (auto- or allochthonous), characterised by different proportions of organic and inorganic matter constituting these particles, as well as in very different sizes, ranging from particles of the submicrometre range, such as colloids and viruses, to particles of the order of hundreds of micrometres in size, such as large plankton cells or sand grains (see, e.g., Stramski et al., 2004). The fact that relationships between the concentration, composition and size distribution of assemblages of particles suspended in water and the optical properties may be generally very complicated, has been demonstrated over the years in numerous theoretical considerations and experimental works. With regard to marine phytoplankton, which is the main optically important autogenic component for the vast majority of surface open ocean areas, examples of works indicating the mentioned complexity include Morel and Bricaud (1986), Bricaud and Morel (1986) or Stramski and Kiefer (1991). Concerning inorganic (mineral) particles, the concentrations of which can be very diverse and therefore important in coastal regions of the oceans, the complexity of their optical properties was indicated, among others, by the following works: Ahn (1999), Babin and Stramski (2004), Stramski et al. (2004) and Stramski et al. (2007).

In this work, we focus on coastal waters found in the Arctic archipelago of Svalbard, which may be an example of optically complex waters, in which there are variable proportions of organic and inorganic components in the water, which is why their optical properties cannot be approximately parameterised only by the concentration of chlorophyll *a*, as is often done for open ocean waters. So far, only a few experimental works have been carried out in this type of water bodies, which would simultaneously document a wide set of inherent optical properties of particles along with concentration measurements, as well as important features of the composition and, at the same time, the sizes of particles suspended in water. Examples of works with such a wide scope include Babin et al. (2003), Peng and Efler (2007), Woźniak et al. (2010), Neukermans et al. (2012), Reynolds et al. (2016) and Woźniak et al. (2018, 2022).

An element necessary for the analyses we intend to carry out in this work is information about the particle size distribution or at least about selected, important features of such a distribution. Relatively commonly used instruments for directly measuring the size distribution of marine suspended particles are resistive pulse sensing counters (Coulter counter), flow imaging microscopy devices (e.g., FlowCAM), or laser diffractometers (e.g., laser in situ scattering and transmissometry devices, LISST-100x or LISST-200x, Sequoia Scientific, Inc.). However, all these instruments have certain limitations. For example, the Coulter counter is generally a laboratory instrument that requires certain minimum stability conditions that are not always possible to be achieved on each of the research vessels during field studies (this was not possible in the case of the research vessel to which the authors of this work had access). In turn, the laser diffractometers (which could be used much easier during field campaigns and in situ) in practice often show the inability to record small-sized particles (smaller than about 2 μm), which are also important to understand and correctly interpret the optical properties of seawater. However, another approach is also possible when trying to practically assess the impact of the size of suspended particles on their optical properties. It involves the physical separation of fractions of different sizes of suspended particles and measuring the optical properties of such isolated fractions. Examples of works in which this approach was used are Ciotti et al. (2002) (documentation of differences in the absorption properties of different size groups of phytoplankton) and Koestner et al. (2020) (documentation of differences in the relationships between particle sizes, composition and optical properties based on laboratory analyses of ocean water samples, mainly from coastal areas).

Inspired by the above examples of the use of physical particle separation (fractionation), our team from the Institute of Oceanology attempted to adapt such methods for use during field research in marine conditions, immediately after collecting water samples. At the same time, we tried to significantly increase the potentially obtainable volumes of fractionated samples to enable a wide spectrum of analyses of the various properties of such samples. The first results obtained using such a modified methodology for the fractionation of large volumes of seawater were presented in the work by Meler et al. (2023), which concerned the absorption properties of size fractions of suspended matter occurring in the Baltic Sea. The next step for our team was to use this modified methodology for the purposes of current work during field research conducted in the Arctic fjords of Spitsbergen.

The aim of this work is to analyse the relationship between selected characteristics of the size distribution of suspended particles, the composition of suspended particles and their optical properties for surface water samples from the optically complex marine environment of fjords and coastal waters of western Spitsbergen. In these analyses, we specifically planned to use the results of direct measurements of samples fractionated according to particle size, obtained by cascade filtration of large volumes

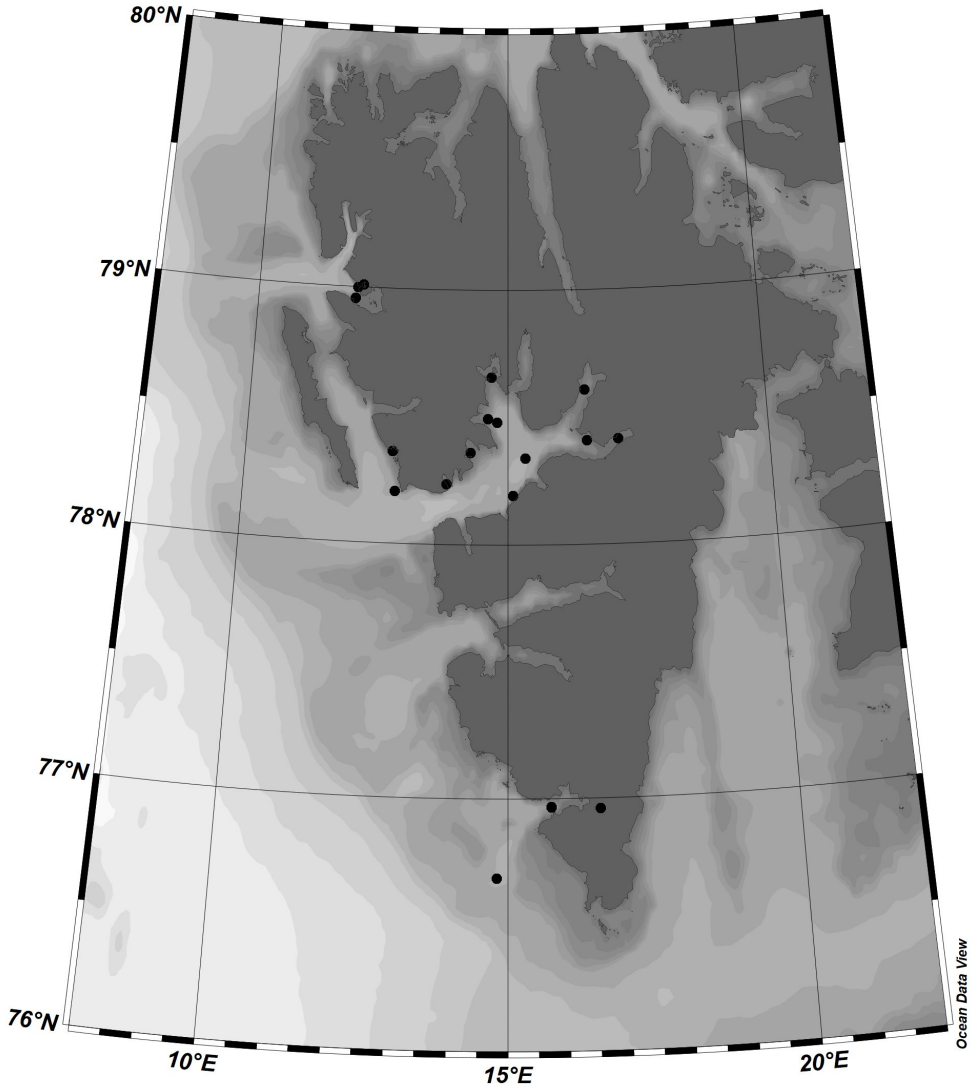

Figure 1. Map with the location of measurement stations in the area of the fjords and the western coast of Spitsbergen (black points represent measurement stations, dark grey colour represents land areas, shades of grey represent bottom bathymetry).

of water samples through a system of meshes and filters with a specific pore size.

2. Material and methods

2.1 Study area and sampling procedures

The research was conducted in selected locations in the fjords and coastal waters of western Spitsbergen, an island belonging to the Arctic archipelago of Svalbard, in the northern part of the Atlantic. Measurements and collection of water samples were carried out during two research expeditions on the r/v *Oceania*, in July and August in 2021 and 2022. The location of the measurement stations is shown in Figure 1. These are selected stations from a larger measurement campaign, from which data were used and analysed in the work by Woźniak et al. (2024), describing the variability of inherent optical properties of seawater in relation to the concentration and composition of suspended particles. In the current work, we use data from selected 19 measurement stations (6 stations from 2021, located within or in the vicinity of the Hornsund fjord (south-western part of the island), in the Isfjord (central part) and the Kongsfjord (northern part of the island); 13 stations from 2022, 12 of them located in the Isfjord area and 1 in the Hornsund fjord). An extended measurement program was carried out at these 19 stations, consisting of fractionating samples according to the size of suspended particulate matter and performing measurements and analyses on both original and fractionated samples.

At each station, large volumes of water (approximately 40–100 L) were collected from the surface layer of sea-

water, using a Niskin bottle or bucket. Immediately after collecting the samples, they were fractionated according to particle size in the ship's laboratory, using filtration methods through meshes and filters with appropriately selected pore sizes. Immediately after these procedures, measurements of the light attenuation coefficient were also performed in the ship's laboratory. After the cruise, measurements of light absorption coefficients by suspended particles, non-algal particles and phytoplankton were made. Several characteristics related to the concentration and composition of suspended particulate matter in the samples were also analysed.

2.2 Fractionation of seawater samples

Fractionation of samples according to particle size was performed using practical procedures developed by our team, which have already been described in detail in the work by Meler et al. (2023). This is an adaptation and modification of the methodology used, among others, by Ciotti et al. (2002) and Koestner et al. (2022). In our case, we used seawater filtration through two types of nylon meshes, with nominal pore sizes of 5 and 20 μm (square pieces, 25 cm × 25 cm, of material used as plankton nets, Hydro-Bios) and through hydrophilic membrane filters (Isopore, 47 mm in diameter, Merck Millipore Ltd.) with a nominal pore size of 2 μm.

Large volumes of seawater collected were mixed in an integration tank, from which a subsample was taken to represent unfiltered seawater (original sample). The remaining volume of water was gravity-filtered through a 20-μm mesh and symbolically designated as fraction A. Then, a subsample required for measurements and analyses was taken from fraction A, and the remaining volume was gravity-filtered through a 5-μm mesh, thus obtaining fraction B. Subsequently, a subsample was taken from fraction B for measurements and analyses, and the remaining volume was filtered through membrane filters with a pore size of 2 μm, under low pressure (< 0.04 MPa). In this way, the last fraction C was obtained.

The original (unfiltered) water sample and the prepared fractions A, B and C were then subjected to the same measurements of optical properties and analyses of the concentration and composition characteristics of suspended matter present in these samples.

The values intended to represent the individual size fractions of suspended particulate matter were obtained in the following way. We considered the results obtained for fraction C to represent very small particles (marked as VS). The remaining size fractions were obtained as appropriate differences in the obtained results. We considered the differences between the results obtained for fraction B and fraction C as representing small particles (S). Differences between results for fraction A and fraction B, as representing medium particles (M). And finally, the differences between the results for the original (unfiltered) water sample and fraction A, as representing large particles (L).

In this work, we consciously define and name the classes distinguished by fractionation as very small (VS), small (S), medium (M) and large (L) particles, and we do not indicate specific size ranges. It is known that fractionation procedures are not able to provide a sharp cut-off of sizes such as those suggested by the size of the meshes or filters used (see, e.g., Koestner et al., 2020). For this reason, it should be understood that the separated size classes are only qualitative in nature.

Additionally, due to the fact that for our water samples the differences between the results for the original sample and fraction A, and often also between fraction A and fraction B, were small or even zero, when presenting most of the results further in this work, we decided to present them for the joint class consisting of medium and large particles together (denoted as ML).

2.3 Concentration, composition and size characteristics of suspended particulate matter

The concentrations of suspended particulate matter, SPM (in units of (g m^{-3})) and its two main fractions, particulate organic matter, POM, and particulate inorganic matter PIM (also in (g m^{-3})), were determined using the combination of standard gravimetric method and the loss-on-ignition technique (Pearlman et al., 1995; see Woźniak et al., 2018 for details). SPM was determined as the dry mass of particles retained by filtration of seawater samples on glass-fibre GF/F filters (25 mm in diameter, Whatman) per unit volume of filtered seawater. PIM was determined as a fraction of particulate mass per unit volume of filtered seawater, which remained on the filters after combustion. POM was determined as a difference between SPM and PIM.

The total concentration of chlorophyll-*a*, Chl*a* (in units of (mg m^{-3})), was obtained as a result of applying high-performance liquid chromatography (HPLC). Details of the HPLC methodology used can be found in Stoń and Kosakowska (2002), Stoń-Egiert and Kosakowska (2005), and Stoń-Egiert et al. (2010). In this paper, we refer to the results of Chl*a* defined as the sum of the concentrations of chlorophyll-*a*-allomer and epimer, chlorophyllide *a*, and phaeophytin *a*.

In the case of the biogeochemical quantities mentioned above, all measurement procedures were carried out both in relation to the original (unfiltered) water samples and fractions A, B and C prepared as a result of filtration. This allowed for the determination of representative values for the size fractions VS, S, M and L. Further, the symbols without subscript denote the values obtained for the original water sample (e.g., SPM, POM, and Chl*a*), while the symbols with subscript correspond to the values for size fractions (e.g., subscript VS for very small particles, and the designations like SPM_{VS}, POM_{VS}, $Chla_{VS}$).

As main characteristics of the general composition of particles suspended in water, we will further use the ratio of POM to SPM, as a representative of the contribution of the organic fraction in the total dry mass of suspended particles, and the ratio of Chl*a* to SPM as a proxy characterizing the contribution of living phytoplankton in the dry mass of suspended particles. We will present such ratios both in relation to the original, unfiltered water samples and to the size fractions (and then these ratios will be marked, for example, as POM_{VS}/SPM_{VS} and $Chla_{VS}/SPM_{VS}$).

As simplified characteristics of particle size distribution in analysed samples we will use the contributions of individual size fractions to total SPM and Chl*a*. Specifically, to describe the relative contributions of particles from different size fractions to the total dry mass of particles we will use the following ratios: SPM_{VS}/SPM, SPM_{S}/SPM and SPM_{ML}/SPM. And in the case of considering living phytoplankton only, we will use the contributions from individual size fractions to the total chlorophyll *a* concentration (the following ratios: $Chla_{VS}$/Chl*a*, $Chla_{S}$/Chl*a* and $Chla_{ML}$/Chl*a*).

2.4 Inherent optical properties

The determination of the spectral beam attenuation coefficient of particles, $c_p(\lambda)$ (in units of (m^{-1})) was made from measurements with a hyperspectral VIS-transmissometer Viper (TriOS). The optical pathlength of this instrument is 15 cm, its nominal spectral range is 350–720 nm, and a spectral measurement interval is about 2 nm. Measurements were performed in a ship's laboratory, immediately after collecting the original and preparation of the fractionated ones, using a special sample chamber provided by the instrument manufacturer, enabling measurements of light transmission on small volumes of samples (300 mL). For each sample, we performed the spectral measurements on a reference 0.2-μm filtered seawater (obtained by filtration through a 0.2-μm pore size cellulose acetate filter; Sartorius Stedim Biotech or Ahlstrom-Munksjö), and on the sample itself. In each case, three replicate spectral scans were made for subsequent averaging. Appropriate attention was paid to avoid bubbles in the samples during measurements. The temperature and salinity of the samples were measured with a portable multi-parametric laboratory meter ('edge HI2003', Hanna Instruments). The correction for the effects of variations in light attenuation of pure water due to changes in temperature and salinity was made using the correction factors according to Ramírez-Pérez et al. (2015). The difference between corrected measurements representing sample, and reference 0.2-μm filtered seawater, was used to calculate attenuation coefficients of particles $c_p(\lambda)$.

We found that a prevailing number of spectra, those exhibiting relatively high values of $c_p(\lambda)$, can be well approximated with a following power function:

$$c_p(\lambda) = c_p(555)\left(\frac{\lambda}{555}\right)^{\eta} \quad (1)$$

The slope coefficient η was fitted using the ordinary least squares (OLS) regression of the relationship between $\log(c_p(\lambda)/c_p(555))$ and $\log(\lambda/555)$. In cases of some measurements, however, when $c_p(\lambda)$ spectra had generally low values, significant noise and deviations from the monotonic spectral behaviour was present. Noise or apparent spectral artefacts were observed mainly for $\lambda < 360$ nm and $\lambda > 650$ nm, and also in the vicinity of 490 nm (potentially it should be attributed to being close to the sensitivity limit of the instrument). For all measured $c_p(\lambda)$ spectra we fitted the power function (Eq. (1)) in the spectral range of 360–650 nm and extrapolated this function for $\lambda < 360$ nm and $\lambda > 650$ nm. We note, however, that in the case of spectra with high overall values, the results of such extrapolation are generally consistent with the "raw" values calculated from direct measurements.

For determinations of spectral absorption coefficients of suspended particulate matter, $a_p(\lambda)$ (in units of (m^{-1})), of depigmented (non-algal) particles, $a_d(\lambda)$ (m^{-1}), and of phytoplankton, $a_{ph}(\lambda)$ (m^{-1}), samples were collected on glass-fibre filters (Whatman GF/F, 25 mm diameter) by filtering between 10 and 500 mL of seawater. The sample filters were immediately flash frozen in liquid nitrogen and stored until post-cruise measurements. Generally, the measurements were made following the protocol recommended in IOCCG (2018). A spectrophotometric filter-pad method was used in configuration in which filters are placed inside the integrating sphere of a spectrophotometer (similar as in Röttgers and Gehnke, 2012; or Stramski et al., 2015). We used the double beam spectrophotometer Lambda 650 (Perkin Elmer) equipped with a 15-cm diameter integrating sphere (Labsphere), and a centre-mounted holder (Perkin Elmer). The spectral scans were made in the 290–860 nm spectral range, at 1 nm intervals. The spectral values of optical density (OD) were measured first on the sample filters after thawing them and then keeping them moistened during the spectral scans. Two replicate scans were made for subsequent averaging. Next, the sample filters were bleached with 0.13% NaClO solution following the method of Tassan and Ferrari (1995, 2002) and rescanned in the spectrophotometer. The measurements of original (untreated) sample filters were used to obtain $a_p(\lambda)$ and the measurements of NaClO-treated filters were used to obtain $a_d(\lambda)$. In turn, $a_{ph}(\lambda)$ was calculated as a difference between $a_p(\lambda)$ and $a_d(\lambda)$. In the process of calculating $a_p(\lambda)$ and $a_d(\lambda)$, the average OD spectrum of the blank filter was subtracted (the average from measurements of several blank filters that were moistened with particle-free seawater). The correction for the pathlength amplification factor was also applied, using the formula according to Stramski et al. (2015), in version for the inside integrating sphere configuration of filter-pad method. Because the phytoplankton absorption coefficient

$a_{ph}(\lambda)$ calculated as a difference between $a_p(\lambda)$ and $a_d(\lambda)$, should be negligible at near-infrared wavelengths (Babin and Stramski, 2002), the measured spectra of $a_d(\lambda)$ were additionally adjusted to ensure than the $a_d(\lambda)$ values in the near-infrared range (800–850 nm) are approximately equal to the measured values of $a_p(\lambda)$ in this range. This adjustment of $a_d(\lambda)$ ensured the null absorption of phytoplankton in the near-infrared. Typically, the needed adjustment of $a_d(\lambda)$ was small and it can be associated with some small changes (other than pigment bleaching itself) in the sample filter induced by subjecting the filter to the NaClO treatment.

Additionally, in this work, a_{ph} spectra for samples with a Chl$a$/SPM ratio equal to or less than 10^{-4} were excluded from further analysis. This value can be considered as the threshold below which experimental determination of $a_{ph}(\lambda)$ by spectrophotometric measurements of samples before and after chemical bleaching or extraction of phytoplankton pigments is highly problematic (Woźniak et al., 2010). For those of our samples that had Chl$a$/SPM below the mentioned threshold, the corresponding a_{ph} spectra did not exhibit typical features of phytoplankton absorption, especially distinct maxima in the blue and red spectral regions.

Having calculated from direct measurements the spectra of $a_p(\lambda)$ and $c_p(\lambda)$, we were also able to estimate the spectra of the total scattering coefficient of particles $b_p(\lambda)$ (m^{-1}), as a difference $c_p(\lambda) - a_p(\lambda)$.

As in the case of determining biogeochemical quantities, also in the case of all the optical quantities mentioned here, all measurement procedures were carried out both in relation to the original (unfiltered) water samples and fractions A, B and C prepared as a result of filtration. This allowed for the determination of optical coefficients representative of size fractions VS, S, M and L. Further in the text, the symbols representing optical properties without subscripts denote the values obtained for the original water sample (e.g., $b_p(\lambda)$, or $a_p(\lambda)$), while the symbols with subcripts correspond to the values for size fractions (e.g., $b_{p,\mathrm{VS}}(\lambda)$, or $a_{p,\mathrm{VS}}(\lambda)$ as coefficients representing fraction VS).

3. Results and discussion

3.1 Concentration, composition and contribution of different size fractions to suspended particulate matter

The collected seawater samples differed significantly in the biogeochemical properties of the suspended particulate matter. Statistics summarizing this variability are presented in Table 1. Comparing the minimum to maximum values, SPM in the original water samples changed more than 31 times, from 0.80 to 25.2 g m^{-3}. Based on measurements in fractionated samples, on average the small particle fraction (S) had the largest contribution to the dry mass of the suspended matter (see Table 1 and Figure 2a). This contribution, described by the $\mathrm{SPM_S}$/SPM ratio, was on average 0.53, and it varied from 0.26 to 0.72. The next

Table 1. Statistics describing the variability of biogeochemical properties of analysed near-surface seawater samples. The table shows SPM and Chl$a$ for particles present in the original, unfiltered seawater samples and the relative contribution of the distinguished particle size fractions (very small (VS), small (S) and combined medium and large (ML)) in these concentrations. In the case of POM/SPM and Chl$a$/SPM ratios, the values presented refer to the original, unfiltered seawater samples and to the size fractions. For each of the quantities presented, the number of analysed samples (n), the average value (Av.) and standard deviation (SD), the coefficient of variation expressed as a percentage (CV), and minimum (Min), median (Med) and maximum (Max) values are provided.

Quantity	n	Av.	SD	CV (%)	Min	Med	Max
SPM (g m^{-3})	19	3.83	5.16	134.9	0.80	3.04	25.2
$\mathrm{SPM_{VS}}$/SPM	19	0.19	0.06	31.7	0.05	0.20	0.32
$\mathrm{SPM_S}$/SPM	19	0.53	0.13	23.6	0.26	0.58	0.72
$\mathrm{SPM_{ML}}$/SPM	19	0.28	0.11	40.5	0.10	0.26	0.52
Chl$a$ (mg m^{-3})	19	0.67	0.37	54.3	0.19	0.65	1.40
$\mathrm{Chl}a_{\mathrm{VS}}$/Chl$a$	19	0.28	0.19	66.5	0.04	0.28	0.97
$\mathrm{Chl}a_{\mathrm{S}}$/Chl$a$	19	0.52	0.18	34.7	0	0.51	0.79
$\mathrm{Chl}a_{\mathrm{ML}}$/Chl$a$	19	0.20	0.18	91.2	0	0.18	0.59
POM/SPM	19	0.27	0.10	37.5	0.10	0.23	0.48
$\mathrm{POM_{VS}}/\mathrm{SPM_{VS}}$	19	0.34	0.14	42.0	0.11	0.33	0.67
$\mathrm{POM_S}/\mathrm{SPM_S}$	19	0.21	0.09	42.7	0.08	0.20	0.46
$\mathrm{POM_{ML}}/\mathrm{SPM_{ML}}$	19	0.32	0.13	40.6	0.15	0.26	0.54
Chl$a$/SPM	19	3.6×10^{-4}	3.8×10^{-4}	105.9	3.5×10^{-5}	2.5×10^{-4}	1.5×10^{-3}
$\mathrm{Chl}a_{\mathrm{VS}}/\mathrm{SPM_{VS}}$	19	4.0×10^{-4}	3.2×10^{-4}	79.3	3.9×10^{-5}	2.8×10^{-4}	1.3×10^{-3}
$\mathrm{Chl}a_{\mathrm{S}}/\mathrm{SPM_S}$	19	4.1×10^{-4}	4.6×10^{-4}	114.7	0	2.2×10^{-4}	1.6×10^{-3}
$\mathrm{Chl}a_{\mathrm{ML}}/\mathrm{SPM_{ML}}$	19	3.5×10^{-4}	5.6×10^{-4}	161.9	0	6.8×10^{-5}	2.4×10^{-3}

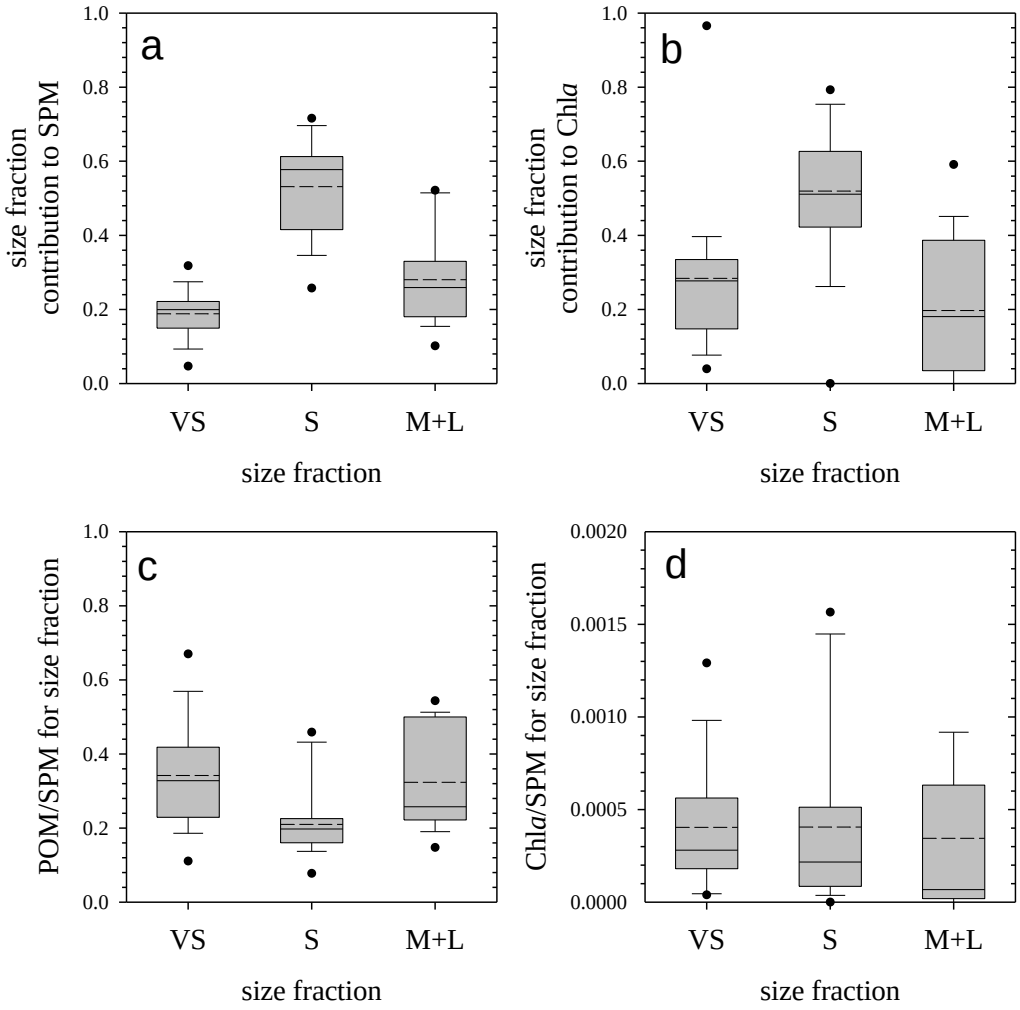

Figure 2. Box plots showing the variability of biogeochemical properties of collected near-surface seawater samples: a) the contribution of V, S and ML size fractions to SPM; b) the contribution of size fractions to Chl*a*; c) POM/SPM ratios for size fractions; d) Chl*a*/SPM ratios for size fractions. Dashed horizontal lines represent the arithmetic averages, solid horizontal lines inside boxes – the medians, outlines of boxes – the 25th and 75th percentiles, whiskers – the 5th and 95th percentiles, black points – non-zero minimum and maximum values.

fraction in terms of average contribution were medium and large particles (ML). Their average contribution (average SPM_{ML}/SPM value) was 0.28, while it varied from 0.10 to 0.52. Very small particles usually had the smallest contribution to SPM. The average SPM_{VS}/SPM value was 0.19, while it varied between 0.05 and 0.32.

In the case of Chl*a*, the observed variability in the original water samples was lower, approximately 7-fold, with values between 0.19 and 1.40 mg m^{-3} (see Table 1 and Figure 2b). On average, the largest contribution to Chl*a*, was the contribution of small particles (S), followed by very small particles (VS) and medium and large particles (ML). These average contributions (average ratios of $Chla_S$/Chl*a*, $Chla_{VS}$/Chl*a* and $Chla_{ML}$/Chl*a*) were 0.52, 0.20 and 0.19, respectively. However, in the case of these contributions, the variability between individual samples was very large, greater than when considering the variability of contribution to SPM. For example, $Chla_S$/Chl*a* describing the contribution of small particles was 0 and 0.79 in extreme cases, and the described variability of this ratio with the coefficient of variation CV (= SD/average value, and expressed in percent) is 34.7%. In the case of the VS fraction, the extreme values are 0.04 and 0.97, and the CV is 66.5%. In the case of the ML fraction, the extreme values are 0 and 0.59, and the appropriate CV is 91.2%.

Considering POM/SPM, i.e. the ratio describing the contribution of the organic fraction to the total dry mass of the suspension, its average values for the original water samples were 0.27, while for the VS, S and ML fractions, they were 0.34, 0.21 and 0.32, respectively (see Table 1

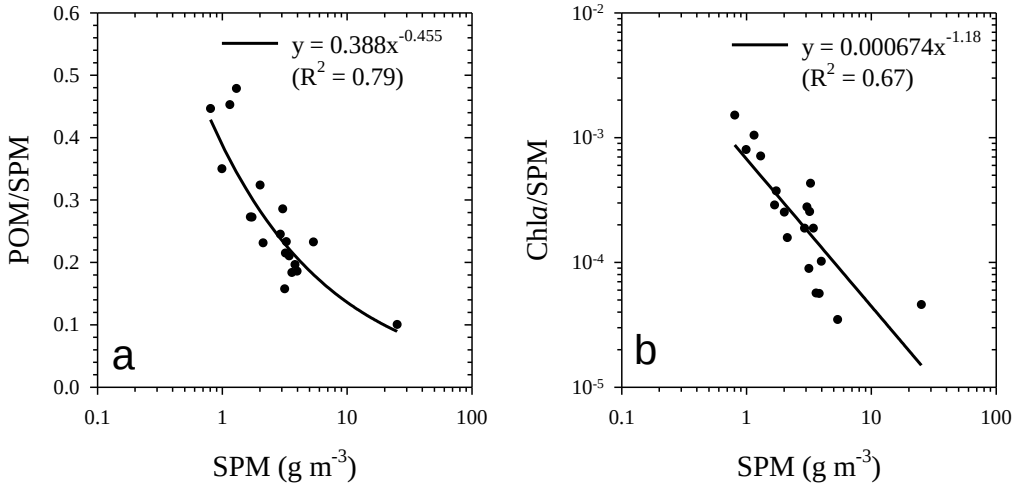

Figure 3. Relationships between the ratios characterizing the composition of suspended particulate matter and its concentration in original, unfiltered seawater samples: a) POM/SPM versus SPM relationship; b) Chl*a*/SPM versus SPM relationship. The points represent individual water samples, the solid lines are the best-fit regression lines whose equations and coefficients of determination R^2 are given in the legends in the individual panels.

and Figure 2c). This means, on average, a lower contribution of the organic fraction in the S size fraction than in the VS and ML fractions. However, these contributions were subject to significant variability between individual samples, which can be illustrated by the values of CVs. For the original samples, it was about 38%, and for the VS, S and ML fractions, about 42, 43 and 41%, respectively.

In turn, the contribution of chlorophyll *a* to the dry mass of the suspended matter, described by Chl*a*/SPM, was very variable. The average for the original samples was 3.6×10^{-4}, and its variability described by the appropriate CV was approximately 106%. Large variability was also observed within the distinguished size fractions. This variability described by the CVs was approximately 79, 115 and 162% for the VS, S and ML fractions, respectively. The VS and S fractions also had slightly higher average values (slightly exceeding 4×10^{-4}) than the ML fraction (3.5×10^{-4}).

For the analysed samples, clear trends of the decrease in the values of POM/SPM and Chl*a*/SPM can also be observed along with the increase in the overall concentration of suspended particulate matter (SPM) in the tested waters. This is confirmed by Figure 3 and the best-fit curves presented therein for the relationship between POM/SPM and SPM, and Chl*a*/SPM and SPM. These are best-fit power functions, obtained using OLS regression method, on appropriately log-transformed input data. They are characterised by high values of the coefficient of determiantion R^2, amounting to 0.79 and 0.67, respectively.

In Figure 4a we present the relationships between

Table 2. Statistics describing the variability of the $b_p(555)$ coefficient, the relative contribution of the VS, S and ML size fractions to $b_p(555)$, and the SPM-specific coefficients $b_p^*(555)$, $b_{p,\mathrm{VS}}^*(555)$, $b_{p,\mathrm{S}}^*(555)$ and $b_{p,\mathrm{ML}}^*(555)$, corresponding to the light scattering by particles in the original samples and in the distinguished size fractions. For each of the characterised quantities, the same statistics are given as in Table 1.

Quantity	n	Av.	SD	CV (%)	Min	Med	Max
$b_p(555)$ (m^{-1})	19	2.25	2.86	127.2	0.41	1.75	14.0
$b_{p,\mathrm{VS}}(555)/b_p(555)$	19	0.25	0.14	56.7	0.05	0.22	0.62
$b_{p,\mathrm{S}}(555)/b_p(555)$	19	0.66	0.15	22.4	0.31	0.68	0.85
$b_{p,\mathrm{ML}}(555)/b_p(555)$	19	0.09	0.12	137.2	0	0.03	0.47
$b_p^*(555)$ $(\mathrm{m}^2\ \mathrm{g}^{-1})$	19	0.615	0.175	28.5	0.303	0.589	0.995
$b_{p,\mathrm{VS}}^*(555)$ $(\mathrm{m}^2\ \mathrm{g}^{-1})$	19	0.829	0.493	59.5	0.300	0.630	2.22
$b_{p,\mathrm{S}}^*(555)$ $(\mathrm{m}^2\ \mathrm{g}^{-1})$	19	0.772	0.267	34.6	0.433	0.737	1.64
$b_{p,\mathrm{ML}}^*(555)$ $(\mathrm{m}^2\ \mathrm{g}^{-1})$	9	0.549	0.452	82.3	0.045	0.364	1.42

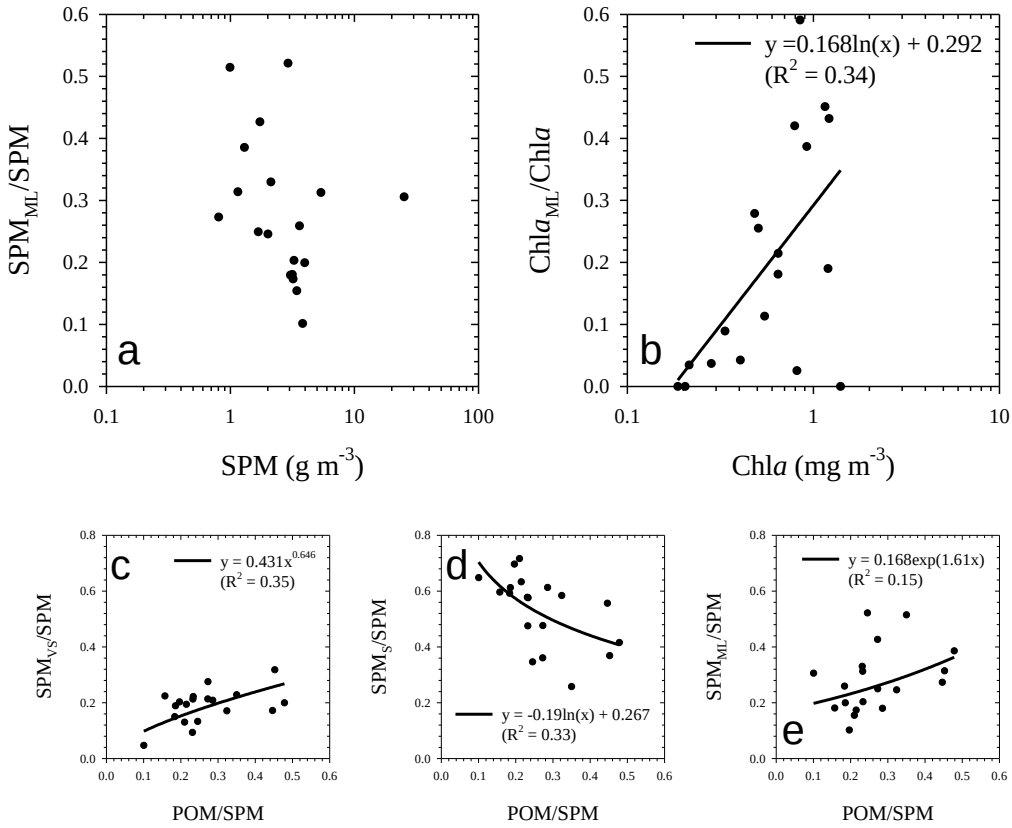

Figure 4. Relationships between selected quantities characterizing the composition and concentration of suspended particulate matter and its distinguished fractions: a) relationship between SPM_{ML}/SPM and SPM; b) relationship between $Chla_{ML}/Chla$ and Chl$a$; c) relationship between SPM_{VS}/SPM and POM/SPM; d) relationship between SPM_S/SPM and POM/SPM; e) relationship between SPM_{ML}/SPM and POM/SPM. The points represent individual water samples, the solid lines in panels b, c, d, and e are the best-fit regressions (appropriate equations and coefficients of determination R^2 are given in the legends).

SPM_{ML}/SPM and SPM for individual water samples. There is no clear correlation here, and we do not present a best-fit curve in this case. The only thing that can be noticed is that for SPM values less than about 3 g m^{-3}, SPM_{ML}/SPM values are usually slightly higher, being above 0.25, while for SPM values greater than 3 g m^{-3}, there are cases of SPM_{ML}/SPM values being less than 0.25.

When analysing the relation between $Chla_{ML}/Chla$ and Chl$a$, we observe a clear tendency to increase the value of the considered ratio with the increase in Chl$a$, which can be approximated by a logarithmic best-fit curve in the form given in the figure, and characterised by the coefficient of determination R^2 of 0.34 (see Figure 4b).

We also draw attention to the observable statistical connection between the variability of the contributions of VS, S and ML fractions to SPM and POM/SPM. This is illustrated in Figure 4c,d,e. With the increase in the POM/SPM value, we observe general statistical trends of an increase in the contributions of the VS and ML fractions and a decrease in the S fraction to SPM. These trends can be approximated by the best-fit power, logarithmic and exponent functions shown in the figure panels.

3.2 Light scattering by particles

Selected characteristics of the scattering coefficient of particles $b_p(\lambda)$ are presented in Figure 5 and Table 2. The values of this coefficient at particular wavelengths of light change for the analysed water samples by more than an order of magnitude (Figure 5a). For example, in the 555 nm band this variability is about 34-fold, with extreme values of 0.41 and 14 m^{-1}. In the considered spectral range from 350 to 720 nm, the contribution of b_p coefficient to the attenuation coefficient of particles c_p varies in extreme cases from 0.75 (for one of the samples in the 350 nm band) to 0.98 (for some of the samples in the 700–720 nm range) (Figure 5b).

The variability of the contribution of size fractions to the b_p coefficient for the exemplary 555 nm band is illus-

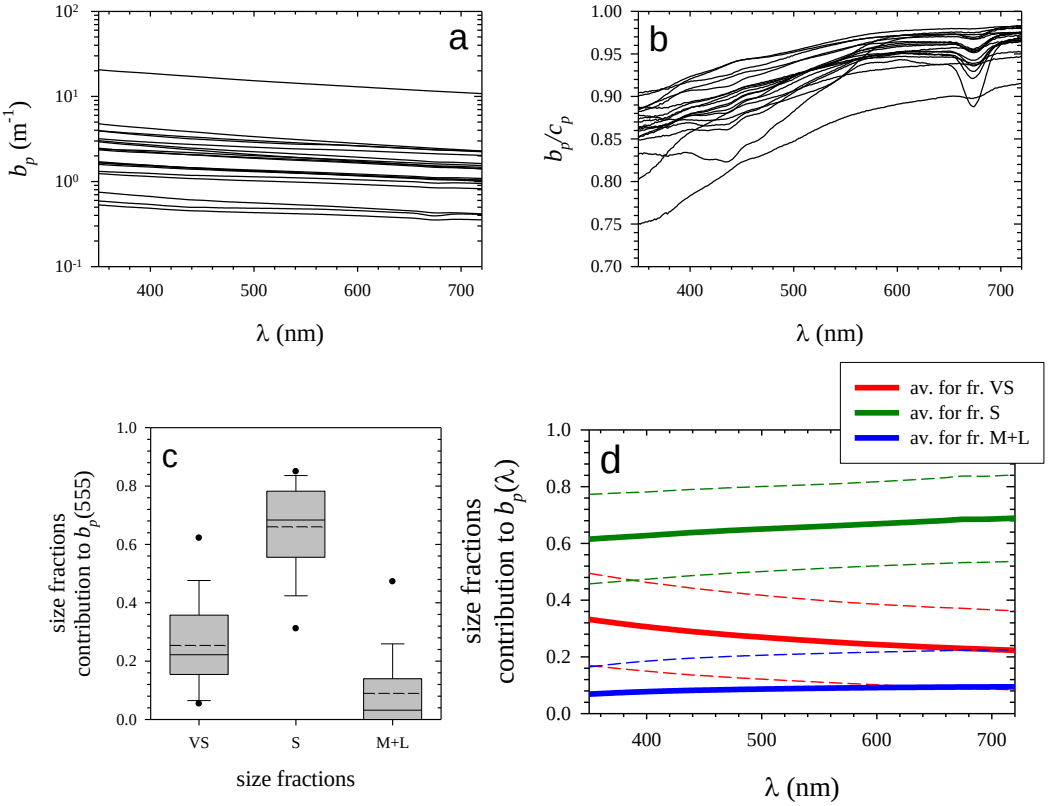

Figure 5. Selected characteristics of light scattering by particles: a) b_p coefficient spectra for individual water samples; b) spectral contribution of the b_p coefficient to c_p; c) boxplots showing the contribution of the VS, S and ML size fractions to $b_p(555)$; d) spectral variability of the average size fraction contributions to b_p (solid lines) with ranges representing the mean ± SD (dashed lines). The colours of the curves represent the VS, S and ML size fractions – see the legend in the panel.

trated in Figure 5c, and the appropriate data are given in Table 2. On average and in most cases, the largest contribution to $b_p(555)$ is made by the S fraction. The average contribution (the average $(b_{p,S}(555)/b_p(555))$ is 0.66 (CV = 22.4%). In extreme cases, this contribution varies from 0.31 to 0.85. The next largest average contribution to $b_p(555)$ is by the VS fraction. Here the average value is 0.25 (CV = 56.7%), and the extreme values are 0.05 and 0.62. The ML fraction makes the smallest contribution on average. It equals 0.09, but the extreme values for this contribution are a minimum of 0 and a maximum of 0.47; the corresponding CV is as high, being approximately 137%.

Similar proportions as for the 555 nm band between the contribution of individual size fractions occur in the entire analysed spectral range in which we were able to determine $b_p(\lambda)$. This is illustrated by the averages and ranges corresponding to the average ± SD for the VS, S and ML fractions, plotted in Figure 5d. However, in relation to the discussed 555 nm band, there is an increase in the average value of the VS fraction contribution for shorter wavelengths, and a decrease in the average contributions for the S and ML fractions (e.g., for 350 nm band the average contributions of S, VS and ML fractions are 0.62, 0.33, and 0.05, respectively).

The analysed b_p spectra for the original water samples also differed to some extent in their slopes, as is illustrated by the Figure 6a and the plotted spectra of the b_p coefficient normalised to its value in the 555 nm band $(b_p(\lambda)/b_p(555))$. To characterize the variability of slopes, we approximated all spectra using an equation of the following form:

$$\frac{b_p(\lambda)}{(b_p(555))} = \left(\frac{\lambda}{555}\right)^{\eta} \tag{2}$$

For the original seawater samples, the mean fitted η value is −0.69 (SD = 0.16).

The spectra of the particle scattering coefficient determined for individual size fractions were also very clearly differentiated. As expected, the spectra for the very small particle fraction (VS) were the steepest on average. The av-

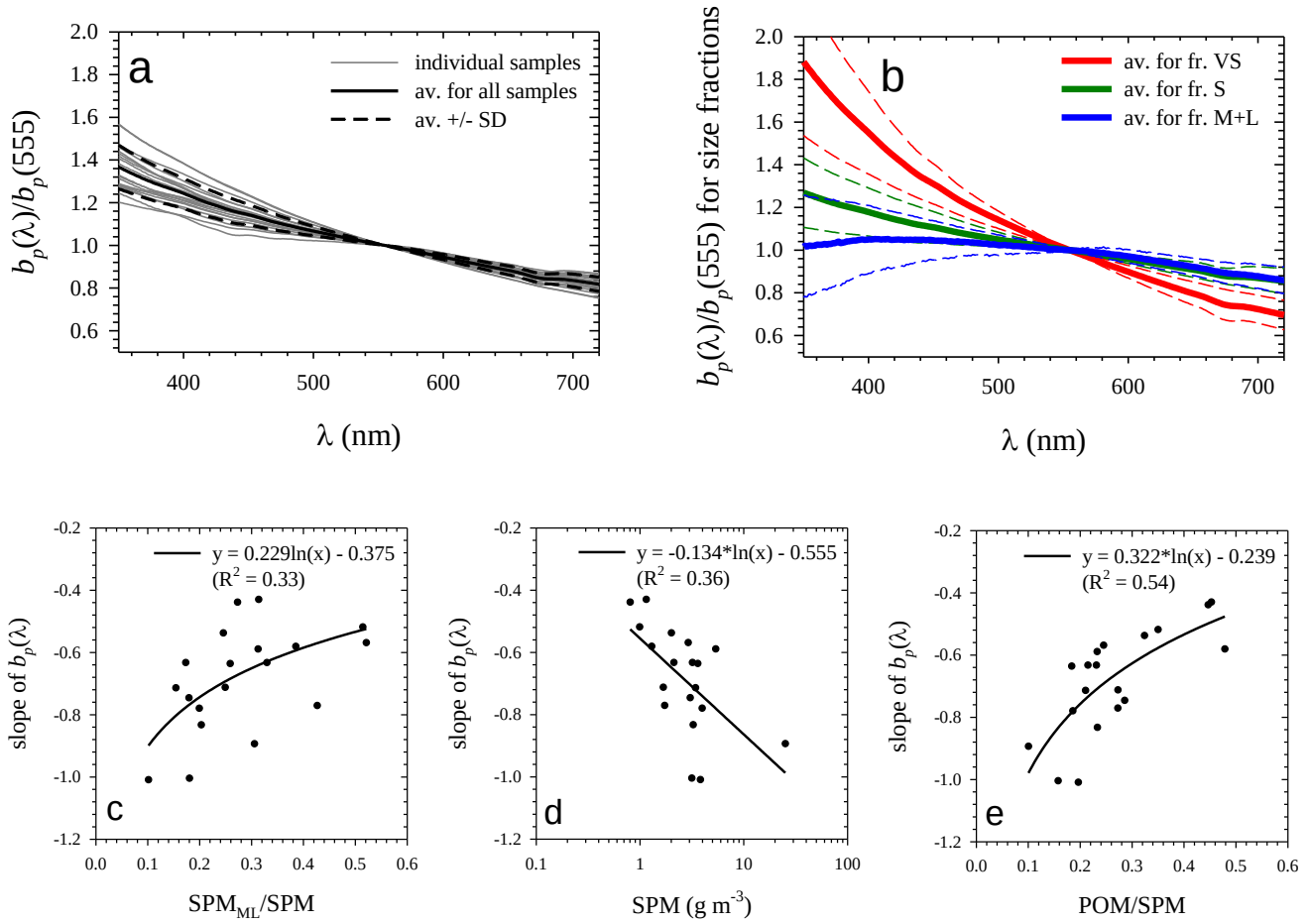

Figure 6. Illustration of the shape variability of the b_p coefficient spectra: a) normalised b_p spectra ($b_p(\lambda)/b_p(555)$) for all samples along with the average normalised spectrum and the range representing the mean $\pm$ SD; b) average normalised b_p spectra for the VS, S, and ML size fractions (solid colour lines) with ranges representing mean $\pm$ SD (dashed colour lines); c) relationship between the slope of the b_p spectra for the original water samples and the contribution of the ML fraction to SPM (SPM_{ML}/SPM); d) relationship between the slope of the b_p spectra and SPM; e) relationship between the slope of the b_p spectra and POM/SPM. See the legends for a description of the line colours in panels a and b. In panels c, d and e, the points represent individual water samples, and the solid lines represent best-fit regressions (appropriate equations and coefficients of determination R^2 are given in the panel legends).

erage slope η of fitted Eq. (2) in this case was -1.34 (SD $=$ 0.38) (see Figure 6b). For the S fraction, the average slope was significantly lower. The mean η is -0.51 (SD $= 0.28$). And the spectra determined for the ML fraction were clearly the flattest. The average η in this case is -0.20 (SD $= 0.40$).

Within the collected data we also observe general statistical trends between the slope of b_p spectra corresponding to the original water samples and selected quantities describing features of the size distribution, as well as concentration and composition of suspended matter. We observe, among others, the relationship between η and SPM_{ML}/SPM, i.e. our size distribution proxy characterizing the contribution of the ML fraction to total SPM (Figure 6c). This relationship can be described by a best-fit regression curve in the form of a logarithmic function:

$$\eta = 0.229 \ln\left(\frac{SPM_{ML}}{SPM}\right) - 0.375 \qquad (3)$$

For this regression the R^2 coefficient is 0.33.

However, we note that η can also be statistically associated with the concentration of suspended particulate matter (SPM) and with the ratio describing the general composition of suspended matter, i.e. POM/SPM. This is illustrated by the best-fit regression curves presented in Figure 6c–d, for which the values of the R^2 coefficient are slightly or significantly higher than R^2 for the above-

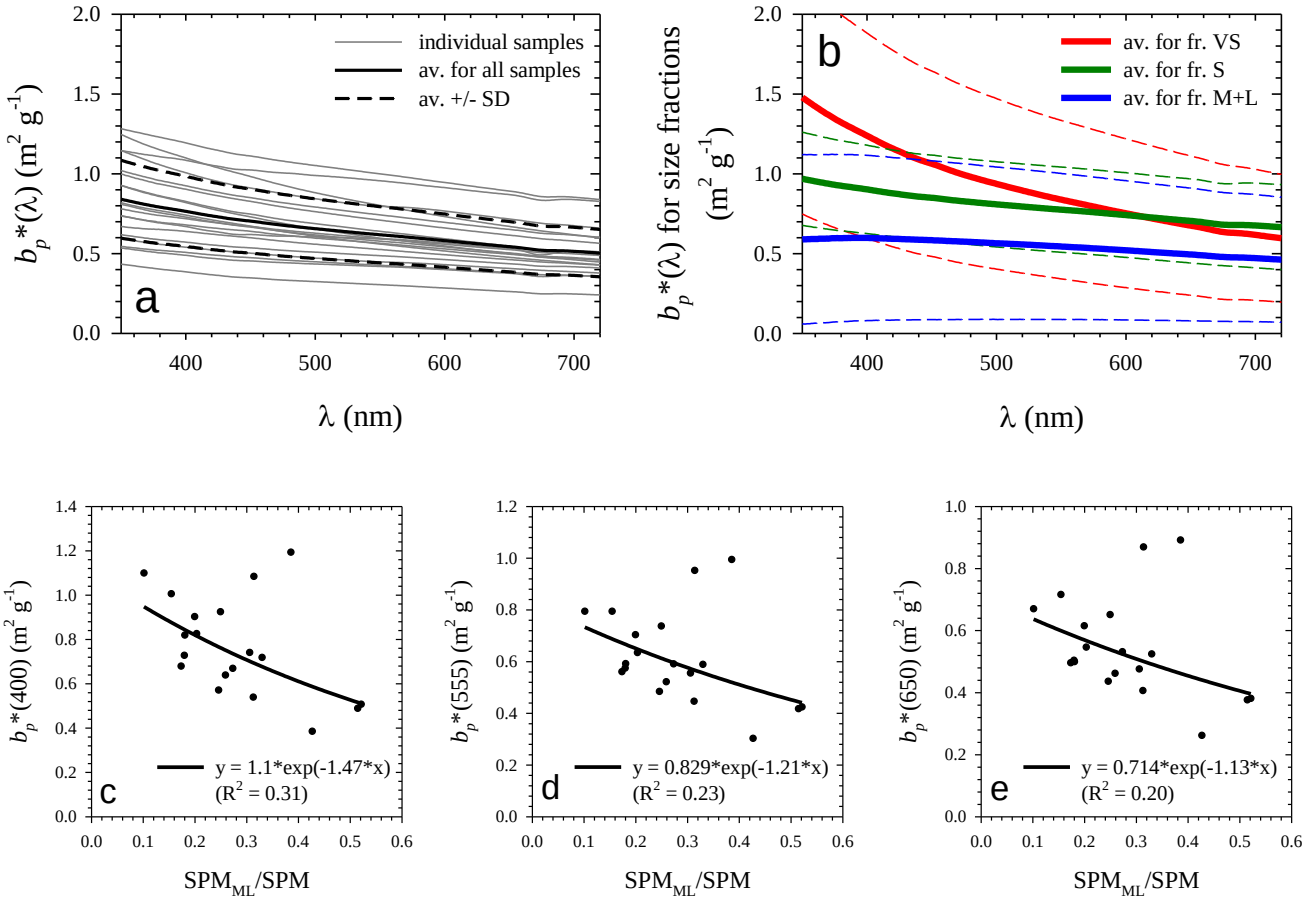

Figure 7. Illustration of the variability of SPM-specific scattering coefficients of particles: a) spectra of SPM-specific coefficient b_p^*, representing individual original, unfiltered samples, together with average spectrum and range representing average ± SD; b) average spectra of SPM-specific coefficients $b_{p,\mathrm{VS}}^*$, $b_{p,\mathrm{S}}^*$ and $b_{p,\mathrm{ML}}^*$ representing size fractions, with ranges representing average ± SD; c) relationship between $b_p^*(400)$ and $\mathrm{SPM_{ML}/SPM}$; d) relationship between $b_p^*(555)$ and $\mathrm{SPM_{ML}/SPM}$; e) relationship between $b_p^*(650)$ and $\mathrm{SPM_{ML}/SPM}$. See the legends in panels a and b for the line colours used. In panels c, d, and e the points represent individual water samples, and the solid lines represent best-fit regressions (appropriate equations are given in the panel legends).

mentioned Eq. (3). $R^2 = 0.36$ for the relationship between η and SPM, and $R^2 = 0.54$ for the relationship between η and POM/SPM.

When analysing the relationship between b_p coefficient and the concentration of suspended particulate matter, we refer to the SPM-specific coefficient $b_p^*(\lambda)(= b_p(\lambda)/\mathrm{SPM})$. Spectral b_p^* values are shown in Figure 7a. Individual samples are characterised by large differences in $b_p^*(\lambda)$. For the 555 nm band the extreme values are 0.303 and 0.995 $\mathrm{m^2\ g^{-1}}$, the average value is 0.615 $\mathrm{m^2\ g^{-1}}$, and the CV is 28.5%.

We also observe a clear differentiation of SPM-specific scattering coefficients of particles when we determine them for individual size fractions. These are symbolically denoted as $b_{p,\mathrm{VS}}^*(\lambda)$, $b_{p,\mathrm{S}}^*(\lambda)$ and $b_{p,\mathrm{ML}}^*(\lambda)$ (where, e.g., $b_{p,\mathrm{VS}}^*(\lambda) = b_{p,\mathrm{VS}}(\lambda)/\mathrm{SPM_{VS}}$). The average values of these coefficients, along with the ranges representing average ± SD, are presented in Figure 7b. For the VS fraction, the average values of $b_{p,\mathrm{VS}}^*(\lambda)$ are the most inclined and, at the same time in the spectral range of light waves smaller than approximately 600 nm, clearly higher than the analogous coefficients for the S and ML fractions. Average $b_{p,\mathrm{S}}^*(\lambda)$ values are intermediate, and average $b_{p,\mathrm{ML}}^*(\lambda)$ values are generally the lowest. In the 555 nm band the average values of the discussed SPM-specific particle scattering coefficients are 0.829, 0.772 and 0.549 $\mathrm{m^2\ g^{-1}}$, respectively (see also the second part of Table 2). However, it should be borne in mind that these coefficients are accompanied by large dispersion of values between individual samples. In the 555 nm band the characteristic CVs are 59.5, 34.6 and 82.3%, respectively.

The observed differences in $b_{p,\mathrm{VS}}^*(\lambda)$, $b_{p,\mathrm{S}}^*(\lambda)$ and

$b^*_{p,\mathrm{ML}}(\lambda)$ coefficients allow us to understand the reasons for the fact that between the values of the SPM-specific coefficient $b_p{}^*(\lambda)$, i.e. the coefficient referring to all particles, and the $\mathrm{SPM_{ML}}$/SPM, we observe statistical trends such as those shown for the 400, 555 and 650 nm bands in Figure 7c–e. In these selected bands we observe a general tendency to decrease the value of $b^*_p(\lambda)$ with an increase in the contribution of particles from the ML fraction to the total dry mass of suspended matter. These trends can be approximated with best-fit regressions in the form of exponential functions:

$$b^*_p(400) = 1.1 \exp\left(-1.47 \frac{\mathrm{SPM_{ML}}}{\mathrm{SPM}}\right) \quad (4)$$

$$b^*_p(555) = 0.829 \exp\left(-1.21 \frac{\mathrm{SPM_{ML}}}{\mathrm{SPM}}\right) \quad (5)$$

$$b^*_p(650) = 0.714 \exp\left(-1.13 \frac{\mathrm{SPM_{ML}}}{\mathrm{SPM}}\right) \quad (6)$$

For these regression curves the R^2 coefficients are 0.31, 0.23 and 0.20, respectively.

3.3 Light absorption by particles and depigmented (non-algal) particles

The spectra of the absorption coefficient of particles, $a_p(\lambda)$, and depigmented (non-algal) particles, $a_d(\lambda)$, are presented in Figure 8a and b. The values of $a_p(\lambda)$ and $a_d(\lambda)$ at individual wavelengths of light change for the analysed water samples by more than an order of magnitude. At the same time, the logarithmic scale for $a_d(\lambda)$ used in Figure 8b allows us to notice that for several samples with low values of this coefficient the phytoplankton pigment bleaching procedure used was not 100% effective (as indicated by visible local maximum values occurring in some

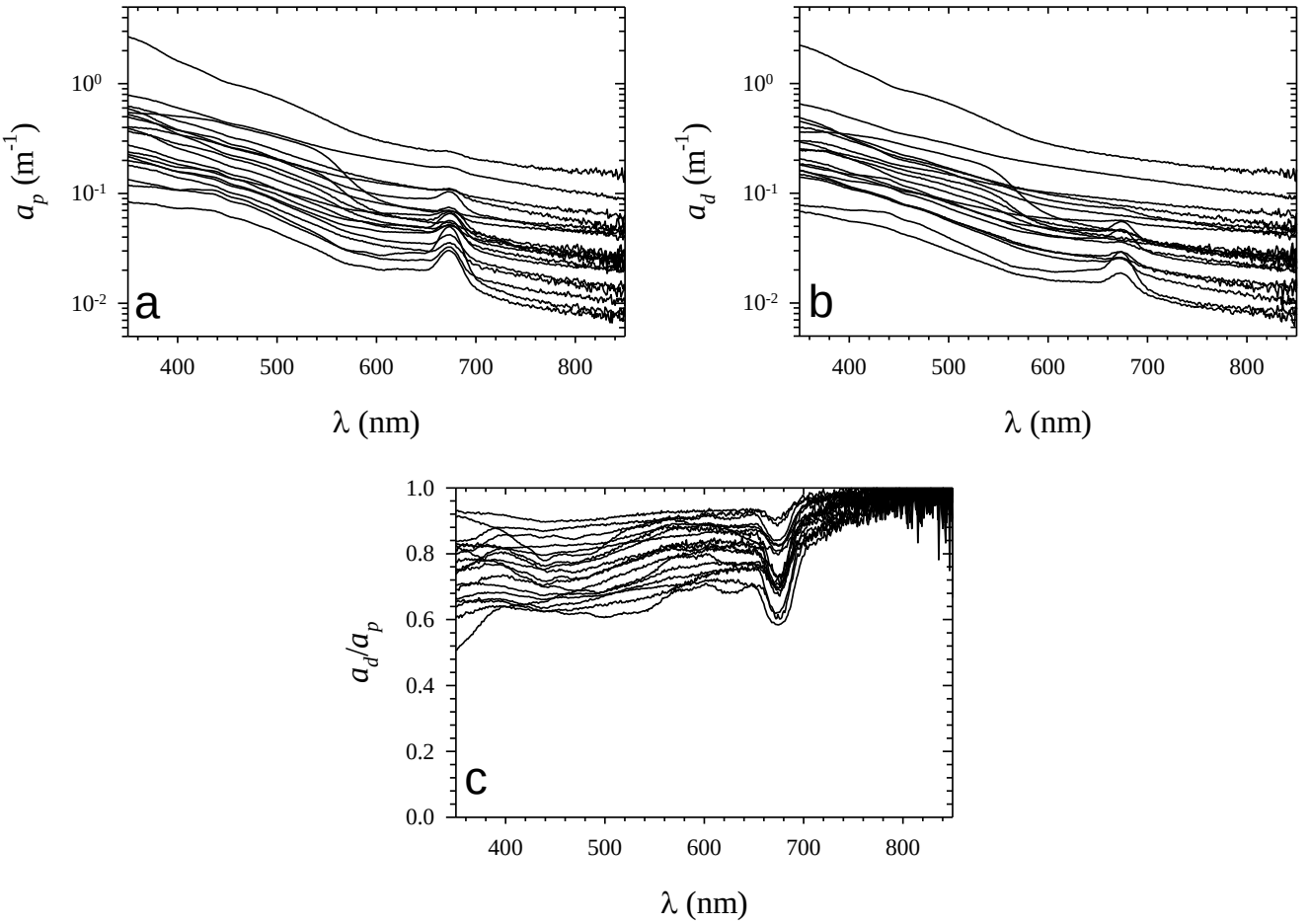

Figure 8. a) a_p coefficient spectra for individual water samples; b) a_d coefficient spectra; c) spectral contribution of the a_d coefficient to a_p.

$a_d(\lambda)$ spectra near the 675 nm band). In the chosen 400 nm band, where $a_p(400)$ and $a_d(400)$ values are generally high, the observed variability is approximately 22-fold and 25-fold, respectively (see Table 3). The extreme values of $a_p(400)$ are 0.073 and 1.61 m^{-1}, while for $a_d(400)$ the extremes are 0.056 and 1.42 m^{-1}. Figure 8c illustrates that the contribution of a_d coefficient to a_p was always substantial, and in most cases and in the whole analysed spectral range, being above 0.6.

The variability of the contribution of size fractions to $a_p(400)$ and $a_d(400)$ are illustrated in Figure 9 a and b, while the statistical data are also given in Table 3. As in the case of the b_p coefficient, on average and in most cases, the largest contributions to $a_p(400)$ as well as to $a_d(400)$ are made by the S fraction of particles. For example, the average value of $a_{p,S}(400)/a_p(400)$ is 0.62 (CV = 19.3%). In extreme cases, this contribution is as little as 0.37 and as much as 0.81. The next highest average contribution to $a_p(400)$ is by the VS fraction. The average value is 0.24 (CV = 31.5%), and extreme values are 0.06 and 0.43. The smallest contribution, on average, to $a_p(400)$ is made by the ML fraction. The average $a_{p,ML}(400)/a_p(400)$ is 0.14. But for this size fraction, the extreme values are 0 and 0.38, and the corresponding CV is 80%. For the $a_d(400)$ coefficient representing depigmented particles the contributions of size fractions are quite similar.

For both, the $a_p(\lambda)$ and $a_d(\lambda)$ coefficients, throughout the whole analysed spectral range, which in this case is 350–850 nm, the contributions of individual size fractions are observed, which are similar to those observed in the case of the $b_p(\lambda)$ coefficient. This is illustrated by the mean values and ranges corresponding to the mean $\pm$ SD for individual size fractions, plotted in Figure 9c–d. For example, the average contribution of fraction S to $a_p(\lambda)$ as well as to $a_d(\lambda)$ through the entire spectral range, roughly vary between 0.6 and 0.7.

The analysed a_p and a_d spectra for the original water samples differed to some extent in their shape. Figure 10 presents the spectral values of the a_p and a_d coefficients normalised normalised to their values in the 400 nm band ($a_p(\lambda)/a_p(400)$ and $a_d(\lambda)/a_d(400)$) along with the mean values and the mean $\pm$ SD ranges. We characterised the variability of a_d slopes (Figure 10b), by approximating all spectra using an equation of the following form:

$$\frac{a_d(\lambda)}{a_d(400)} = \exp(S_d(\lambda - 400)) \tag{7}$$

When fitting with Eq. (7) was performed for a range of wavelengths between 350 and 650 nm (to avoid artefacts occurring around the 675 nm band), the mean fitted S_d value turned out to be -0.0049 (SD = 0.0008). For the a_p and a_d coefficient we did not note systematic differences in shapes for individual size fractions.

To describe the relationships between a_p or a_d and the concentration of suspended particulate matter, we refer to the SPM-specific coefficients: $a_p^*(\lambda)(= a_p(\lambda)/\mathrm{SPM})$ and $a_d^*(\lambda)(= a_d(\lambda)/\mathrm{SPM})$. The spectra of $a_p^*(\lambda)$ and $a_d^*(\lambda)$ for individual samples are shown in Figure 11a–b. Individual samples are characterised by large differences in $a_p^*(\lambda)$ and $a_d^*(\lambda)$ values. For the 400 nm band the observed extreme values of $a_p^*(400)$ are 0.062 $m^2\ g^{-1}$ and 0.188 $m^2\ g^{-1}$, the average value is 0.101 $m^2\ g^{-1}$, and CV is 33.3%. For the $a_d^*(400)$ the extremes are 0.041 $m^2\ g^{-1}$ and 0.153 $m^2\ g^{-1}$, while the average is 0.079 $m^2\ g^{-1}$.

Some differences are also observed between SPM-specific absorption coefficients by particles and depigmented (non-algal) particles defined for individual particle size groups. Average spectral values of sets of coefficients symbolically marked as $a_{p,VS}^*(\lambda)$, $a_{p,S}^*(\lambda)$, $a_{p,ML}^*(\lambda)$ and $a_{d,VS}^*(\lambda)$, $a_{d,S}^*(\lambda)$, $a_{d,ML}^*(\lambda)$ (where, e.g., $a_{p,VS}^*(\lambda) = a_{p,VS}(\lambda)/\mathrm{SPM}_{VS}$), along with the ranges representing average $\pm$ SD, are shown in Figure 11c–d. For both these sets of coefficients, representing different size groups of either untreated or depigmented particles, we observe slightly higher average values for the VS and S fractions, and slightly lower for the ML fraction, which is visible mostly in the shortwave part of the analysed spectral range. For example, in the 400 nm band the average values of the set of coefficients representing size fractions of untreated particles, $a_{p,VS}^*(400)$, $a_{p,S}^*(400)$ and $a_{p,ML}^*(400)$, are 0.130, 0.123 and 0.061 $m^2\ g^{-1}$, respectively (see the second part of Table 3). However, these coefficients are accompanied by large dispersion of values between individual samples. In the 400 nm band the appropriate coefficients of variation (CV) are 33.7, 39.1 and 79.7%, respectively. Similar relationships occur for the set of coefficients representing size fractions of depigmented particles, i.e. for $a_{d,VS}^*(400)$, $a_{d,S}^*(400)$ and$a_{d,ML}^*(400)$ (see data given in Table 3).

The observed differences in the average values of the analysed above sets of SPM-specific coefficients, specified for the distinguished size fractions of either untreated or depigmented particles, understandably may translate into the facts that between the SPM-specific coefficient referring to all untreated or depigmented particles, $a_p^*(\lambda)$ or $a_d^*(\lambda)$, and $\mathrm{SPM}_{ML}/\mathrm{SPM}$, we should also observe statistical trends. However, these trends seem to be weaker than the trends observed earlier in the case of $b_p^*(\lambda)$ vs $\mathrm{SPM}_{ML}/\mathrm{SPM}$ relationships. Figure 11e–f illustrate the relationships between $a_p^*(400)$ or $a_d^*(400)$ and $\mathrm{SPM}_{ML}/\mathrm{SPM}$. These relations can be approximated by the best-fit lines represented by the following exponential functions:

$$a_p^*(400) = 0.138\ \exp\left(-1.27\ \frac{\mathrm{SPM}_{ML}}{\mathrm{SPM}}\right) \tag{8}$$

$$a_d^*(400) = 0.102 \exp\left(-1.11\ \frac{\mathrm{SPM}_{ML}}{\mathrm{SPM}}\right) \tag{9}$$

However, for these regression curves the R^2 coefficient is relatively low and amounts to only 0.21 or 0.16. And for

Table 3. Statistics describing the variability of $a_p(400)$ and $a_d(400)$ coefficients, the relative contributions of the VS, S and ML size fractions to $a_p(400)$ and $a_d(400)$, and the SPM-specific coefficients (marked by '*' symbols), corresponding to the light absorption by particles or depigmented (non-algal) particles in the original samples and in the distinguished size fractions. For each of the characterised quantities, the same statistics are given as in Table 1.

Quantity	n	Av.	SD	CV (%)	Min	Med	Max
$a_p(400)$ (m^{-1})	19	0.34	0.33	97.4	0.073	0.259	1.61
$a_{p,VS}(400)/a_p(400)$	19	0.24	0.08	31.5	0.06	0.23	0.43
$a_{p,S}(400)/a_p(400)$	19	0.62	0.12	19.3	0.37	0.60	0.81
$a_{p,ML}(400)/a_p(400)$	19	0.14	0.11	80.0	0	0.08	0.38
$a^*_p(400)$ ($m^2\ g^{-1}$)	19	0.101	0.034	33.3	0.062	0.091	0.188
$a^*_{p,VS}(400)$ ($m^2\ g^{-1}$)	19	0.13	0.044	33.7	0.076	0.13	0.22
$a^*_{p,S}(400)$ ($m^2\ g^{-1}$)	19	0.123	0.048	39.1	0.074	0.099	0.227
$a^*_{p,ML}(400)$ ($m^2\ g^{-1}$)	15	0.061	0.049	79.7	0.011	0.042	0.214
$a_d(400)$ (m^{-1})	19	0.27	0.29	108.1	0.056	0.208	1.42
$a_{d,VS}(400)/a_d(400)$	19	0.27	0.08	29.0	0.06	0.26	0.44
$a_{d,S}(400)/a_d(400)$	19	0.65	0.13	19.5	0.33	0.66	0.80
$a_{d,ML}(400)/a_d(400)$	19	0.08	0.12	136.7	0	0.04	0.40
$a^*_d(400)$ ($m^2\ g^{-1}$)	19	0.079	0.027	34.6	0.041	0.068	0.153
$a^*_{d,VS}(400)$ ($m^2\ g^{-1}$)	19	0.114	0.036	31.9	0.058	0.112	0.181
$a^*_{d,S}(400)$ ($m^2\ g^{-1}$)	19	0.098	0.038	39.3	0.055	0.088	0.194
$a^*_{d,ML}(400)$ ($m^2\ g^{-1}$)	9	0.056	0.058	103.5	0.009	0.027	0.196

longer light wavelengths, the observed trends are getting even weaker.

3.4 Light absorption by phytoplankton estimated for a limited number of samples

The selected characteristics of the a_{ph} coefficient we were able to obtain based on our current data are presented in Figure 12 and Table 4. Figure 12a shows spectra of the a_{ph} coefficient calculated based on measurements of a_p and a_d, for 12 out of 19 water samples analysed in this paper, which were left after the application of the criterion mentioned in the methodological section (i.e. after exclusion from the analyses of the a_{ph} spectra calculated for samples with a Chl$a$/SPM ratio $<= 10^{-4}$). For such a limited set of samples, the a_{ph} coefficient at particular wavelengths of light changes by more than 6 times. For example, the extreme values recorded in the 440 nm band are 0.0234 and 0.153 m^{-1}. As for the contribution of the a_{ph} coefficient to the absorption coefficient of particles a_p, it varied for the samples considered from below 0.1 to a maximum of 0.4 (which was already indirectly documented by Figure 8c, presenting the contribution of a_d coefficient to a_p).

The variability of the contribution of size fractions to $a_{ph}(440)$ for the limited set of samples is illustrated in Figure 12b. Generally, if we consider the average contributions of individual size fractions, the order of average values is similar to that of the b_p or a_p and a_d coefficients discussed earlier. However, the average values themselves and the proportions between them are slightly different. For the S fraction the contribution to $a_{ph}(440)$ is still the highest on average, and in this case the average is 0.51 (CV= 47.7%). However, this is a clearly lower average than the values of 0.66, 0.62 and 0.65 that we recorded in the case of contribution to the $b_p(555)$, $a_p(400)$ and $a_d(400)$ coefficients. In extreme cases, $a_{ph,S}(440)/a_{ph}(440)$ is as low as 0 and as high as 0.87. As for the average contribution of the VS fraction, it is 0.26 (CV= 54.5%), and the extreme values are 0.13 and 0.63. In the case of the ML

Table 4. Statistics describing the variability of the $a_{ph}(440)$ coefficient and the relative contribution of the VS, S and ML size fractions to $a_{ph}(440)$, specified for the limited number of samples. For each of the characterised quantities, the same statistics are given as in Table 1.

Quantity	n	Av.	SD	CV (%)	Min	Med	Max
$a_{ph}(440)$ (m^{-1})	12	0.0633	0.0408	64.5	0.0234	0.0452	0.153
$a_{ph,VS}(440)/a_{ph}(440)$	12	0.26	0.14	54.5	0.13	0.21	0.63
$a_{ph,S}(440)/a_{ph}(440)$	12	0.51	0.24	47.7	0	0.46	0.87
$a_{phML}(440)/a_{ph}(440)$	12	0.23	0.23	103.3	0	0.18	0.56

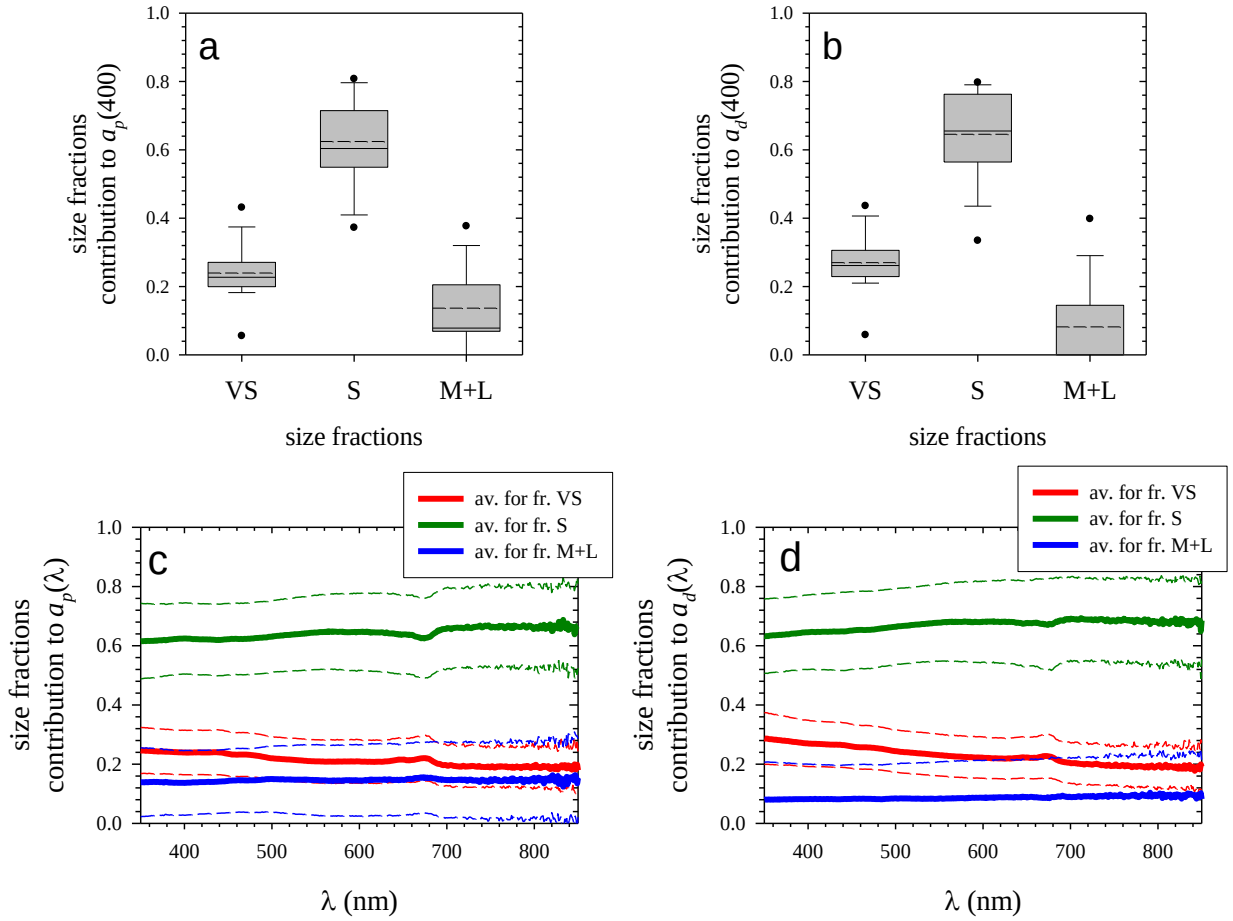

Figure 9. a) and b) boxplots showing the variability of the contribution of the VS, S and ML size fractions to $a_p(400)$ and $a_d(400)$; c) and (d) spectral variability of the average size fraction contributions to $a_d(\lambda)$ or $a_d(\lambda)$ (solid lines) with ranges representing the average $\pm$ SD (dashed lines). For colours used to represent fractions VS, S and ML, see the legends in the panels.

fraction, the average contribution is slightly lower, amounting to 0.23 (CV= 103.3%). The extreme values are 0 and 0.56.

Similar contributions of individual size fractions to the a_{ph} coefficient are observed in the entire analysed spectral range, which in this case is from 350 to 750 nm, as illustrated in Figure 12c. For the limited data on the $a_{ph}(\lambda)$ coefficient, we can note firstly, that greater differences are observed between individual samples, and secondly, on average, particles from the ML fraction usually have a slightly larger contribution, while particles from the S fraction have a slightly smaller contribution, than in the cases of coefficients $b_p(\lambda)$ or $a_p(\lambda)$ and $a_d(\lambda)$.

The analysed a_{ph} spectra for the original water samples from our limited data set differ in their shape. It is illustrated in Figure 12d, presenting the spectral values of the a_{ph} coefficient normalised to its value in the 440 nm band ($a_{ph}(\lambda)/a_{ph}(440)$). While all of the spectra show a clear peak in the 675 nm band, only some of them show a peak in the 440 nm band. For the a_{ph} coefficient we also note some noticeable differences in the average of normalised coefficients calculated for individual size fractions, as illustrated in Figure 12e. The average shape of $a_{ph}(\lambda)/a_{ph}(440)$ for the VS fraction clearly shows that in these particular spectra there is a distinct local peak in the 440 nm band. This peak gradually disappears when we move to the average for the S fraction and then to the average for the ML fraction.

Mainly due to the limited number of reliable data obtained here, representing the absorption by phytoplankton by different size fractions, we decided not to present the analyses of the $a_{ph}(\lambda)$ versus Chl*a* or other biogeochemical factors. However, we can refer interested readers to a separate paper (see Woźniak et al., 2024), in which we present this type of analysis in relation to original (unmodified) seawater samples, based on empirical material collected on a larger number of sampling station in the Arctic fjords of Spitsbergen.

3.5 Comparison with selected results from the literature

The results obtained for samples from Arctic coastal waters around Spitsbergen presented in the preceding sections can now be briefly compared with selected results from the literature. The main purpose of the short comparison made here is primarily to indicate how different marine environments, which all are generally classified as optically complex environments, also referred to as 'case 2 waters', can be in terms of the composition, optical properties, as well as contributions of various size fractions to the biogeochemical and optical properties of suspended particulate matter.

The results concerning the composition and contribution of different size fractions to main biogeochemical quantities describing suspended particulate matter, presented earlier, among others, in Table 1 and Figure 2, can be compared with the results recently obtained by Meler et al. (2023) for the waters of the southern Baltic Sea. Importantly, as we already mentioned, the results of Meler et al. were obtained using identical methods of sample fractionation and light absorption measurements but were carried out on water samples from both nearshore and offshore locations in the southern Baltic Sea. For their samples, Meler et al. (2023) measured or determined the following values: the average contributions to SPM from different size fractions, marked according to the nomenclature from this study as VS, S, M and L, amounting to 0.27, 0.26, 0.28 and 0.17, respectively (the summed contribution representing the M and L fractions together being equal 0.45); the average contributions to Chl*a* of the VS, S, M and L size fractions being of about 0.33, 0.33, 0.15 and 0.18, respectively (the summed contribution of M and L fractions being equal 0.33). This confirms that in the Arctic waters we are dealing with in this paper, a much higher contribution of the S fraction is observed, compared to the samples from the southern Baltic Sea analysed by Meler et al. As for the ratios describing the composition of particles in original samples and for individual size fractions of particulate matter, Meler et al. obtained the following: the average POM/SPM value for original, unmodified samples amounting to 0.58, and for VS, S, M and L size fractions, the values of 0.63, 0.72, 0.59 and 0.53, respectively; the average value of the Chl*a*/SPM ratio for unmodified samples of 1×10^{-3}, and for the VS, S, M and L fractions, the values of 2.6×10^{-3}, 3.7×10^{-3}, 7×10^{-4} and 1.1×10^{-3}, respectively. This generally means that in the case of the Arctic fjord waters we are dealing with, there is a distinct domination of inorganic fraction of suspended particulate matter, and a significantly lower contribution of living phytoplankton in all analysed particle size fractions, compared to the waters of the southern Baltic Sea studied by Meler et al. This, of course, has consequences for the optical properties of suspended matter in these various water basins.

Referring to the results regarding the scattering of light by particles, we can first recall the work of Davies et al. (2014), in which the authors performed modelling based on Mie theory. They assumed two types of spherical particles intended to represent in a simplified way a typical phytoplankton assemblages or typical inorganic particle assemblages suspended in seawater. They also assumed the potential variability of slopes of the power-law size distribution of suspended particles (Junge distribution), i.e. the variability between extreme values of -3.5 and -4.5. Their calculations were performed for light with a wavelength of 532 nm. Davies et al., among others, determined the curves representing the so-called cumulative scattering, expressing the contribution of particles of par-

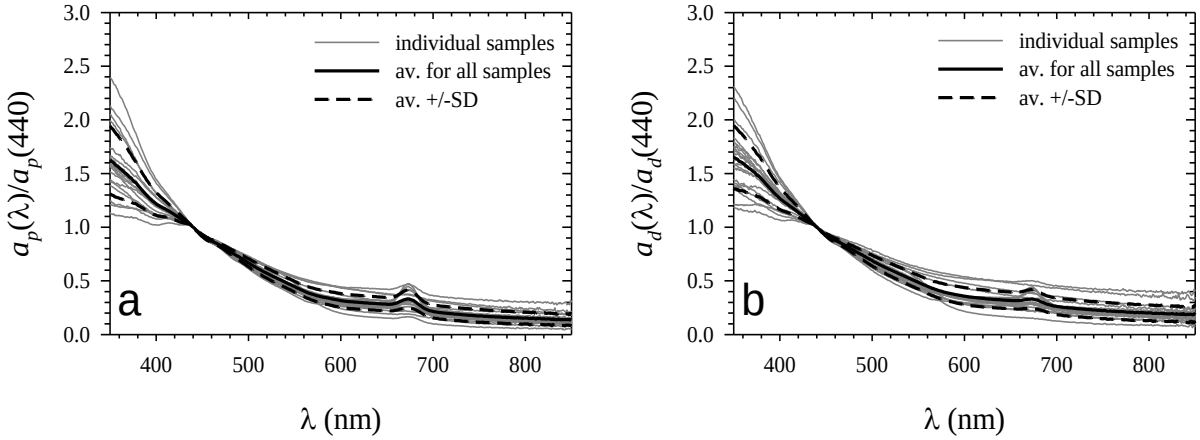

Figure 10. Normalised spectra of a) a_p ($a_p(\lambda)/a_p(400)$) or b) a_d ($a_d(\lambda)/a_d(400)$), for all individual samples together with average normalised spectra and ranges representing averages $\pm$ SD (for line descriptions, see the legends in the panels).

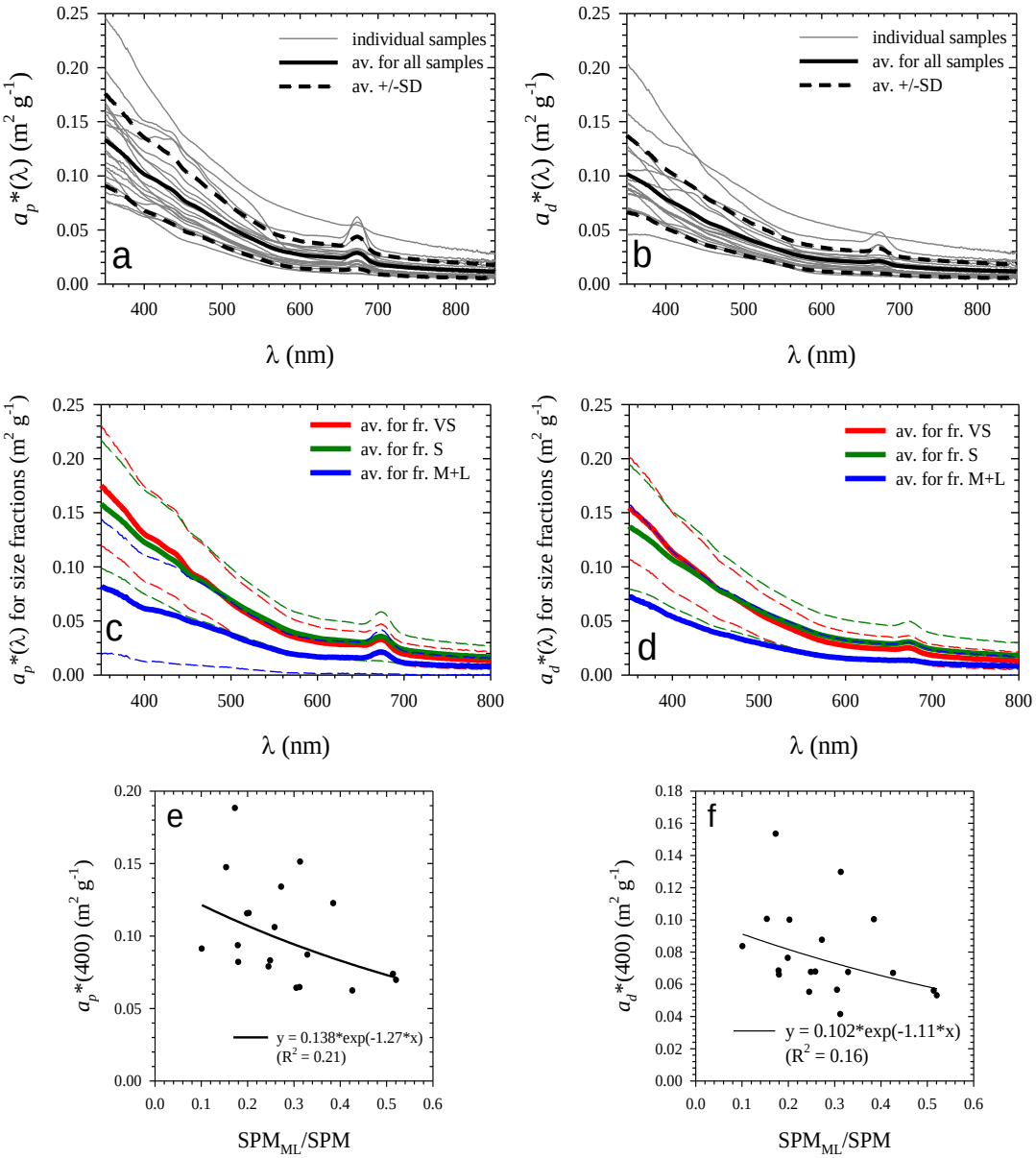

Figure 11. Illustration of the variability of SPM-specific absorption coefficient of particles and depigmented (non-algal) particles: a) and b) spectra of SPM-specific coefficients a_p^* and a_d^*, representing individual either original, unfiltered or depigmented samples, together with average spectra and ranges representing average $\pm$ SD; c) average spectra of SPM-specific coefficients $a_{p,\mathrm{VS}}^*$, $a_{p,\mathrm{S}}^*$ and $a_{p,\mathrm{ML}}^*$ representing size fractions, with ranges representing average $\pm$ SD; d) average spectra of SPM-specific coefficients $a_{d,\mathrm{VS}}^*$, $a_{d,\mathrm{S}}^*$ and $a_{d,\mathrm{ML}}^*$ with ranges representing average $\pm$ SD; e) relationship between $a_p^*(400)$ and $\mathrm{SPM_{ML}/SPM}$; f) relationship between $a_d^*(400)$ and $\mathrm{SPM_{ML}/SPM}$. See the legends in panels a, b, c and d for line colours. In panels e and f, the points represent individual water samples, and the solid lines represent the best-fit regressions (the appropriate equations are given in the panel legends).

ticular sizes to the light scattering coefficient $b_p(532)$. By reading the data from the plots presented by Davies et al. (2014), it can be seen that the estimated contribution to $b_p(532)$ of particles with sizes no larger than 5 μm should be between approximately 70% and 98% (with slightly lower values estimated to represent the possible contribution from phytoplankton particles and slightly higher for mineral particles). Secondly, we can also refer to the percentage contribution of different size fractions to $b_p(532)$, determined as a result of fractionation and measurements

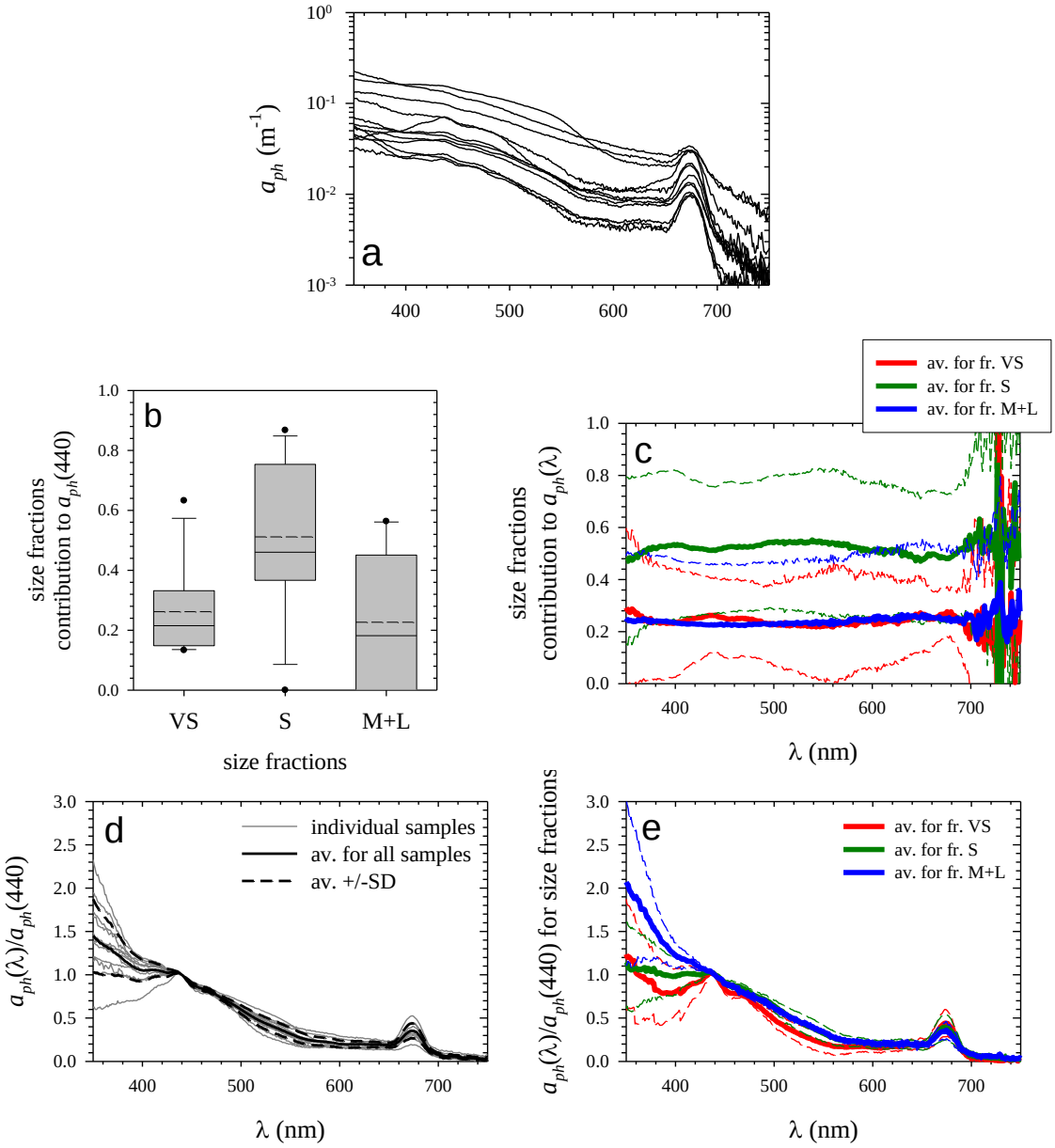

Figure 12. Selected characteristics of light absorption by phytoplankton, obtained for a limited number of samples: a) a_{ph} coefficient spectra for individual samples; b) boxplots showing the contribution of the VS, S and ML size fractions to the $a_{ph}(440)$; c) spectral variability of the average size fraction contributions to the a_{ph} (solid lines) with ranges representing the average $\pm$ SD (dashed lines) (for colours of the curves representing different size fractions – see the legend in the panel); d) normalised a_{ph} spectra ($a_{ph}(\lambda)/a_{ph}(440)$) for individual samples along with the average normalised spectrum and the range representing the average $\pm$ SD; e) average normalised a_{ph} spectra for the VS, S, and ML size fractions (solid lines) with ranges representing average $\pm$ SD (dashed lines) (for colours used, see the legend).

performed on natural water samples, described by Koestner et al. (2020). The results presented by these authors allow us to estimate the percentage contribution from particles defined by us in this work as the sum of the VS and S fractions. We can quote some of the results of Koestner et al., which correspond directly to measurements of samples subjected to physical fractionation of particles, and not yet corrected for the effects of filtering imperfections (which is similar to what we report in this work). For water samples from the San Diego River estuary, Koestner et al. found

the contributions to $b_p(532)$ from the VS and S fractions of particles to be about 28% or 35%; for water samples taken at the pier at Scripps Institution of Oceanography – being about 46%, 55%, 67% or 90%; and finally, for the offshore water samples from different depths – being about 71% or 84%. We note that for the samples analysed in this work, the contribution from particles belonging to the VS and S fractions to the $b_p(532)$ is on average 91% (arithmetic mean); the extreme values for individual samples were 53% and 100%, and the values corresponding to the 1st quantile, the median and the 3rd quantile of the set of our 19 samples are 86%, 97% and 100%, respectively. In this sense, our results indicate a greater contribution of particles <= 5 μm to the $b_p(532)$ coefficient than the approximate and simplified predictions according to Davies et al. (2014), but at the same time our results overlap to some extent with the wide range of values indicated by the measurement of Koestner et al. (2020). This proves, first of all, the possible large variation in the contribution of particles <= 5 μm to the scattering of light in various marine waters, with various suspended particulate matter assemblages of different origin and composition.

Referring to the results regarding the absorption of light by particles, let us point to just one example, documenting again that the average values obtained for the suspended matter samples from Arctic coastal waters distinctively differ from the waters of the southern Baltic Sea studied by Meler et al. (2023). According to data from Meler et al., the contribution of the VS, S, M and L size fractions to the $a_p(443)$ coefficient for the southern Baltic Sea is on average 33%, 37%, 22% and 8%, respectively (the summed contribution of the M and L fractions being 30%). For our samples, the average contribution to $a_p(443)$ for the equally defined size fractions is 24%, 62%, 7% and 7%, respectively (the summed contribution of the M and L fractions being 14%). This proves, among other things, the characteristically high contribution to light absorption, coming from the S fraction in the Arctic fjord waters we studied, which are dominated by the presence of the inorganic fraction of particles.

The few examples of comparisons presented above indicate the differences in the biogeochemical and optical properties of various particle size fractions occurring between different coastal marine environments. This suggests, among others, the possibility and desirability of focusing on future comparative work that will document these types of differences more precisely. This will definitely help to achieve better interpretation of the role of variability in particle size distribution and particle biogeochemical composition in various coastal, optically complex marine environments.

4. Summary and final remarks

As a summary, we would like to remind the reader that the results presented in this article, obtained based on measurements carried out on fractionated seawater samples, should be treated primarily as qualitative, and not strictly quantitative results. This is due to the imperfect ability to separate particles of selected sizes by filtering (see, e.g., a discussion in Koestner et al., 2020). Nevertheless, the obtained results: (i) indirectly indicate a clear variability in particle size distributions occurring in the studied marine environment; (ii) indicate noticeable differences in composition between the distinguished size fractions; (iii) in most cases indicate that the fraction S had the largest contribution to all analysed spectral optical coefficients, followed by the VS and ML fractions; (iv) allowed for the identification of statistical relationships between the selected characteristic describing changes in particle size (the $\mathrm{SPM_{ML}}$/SPM ratio) and variability of particle IOPs. More details on these four main observations are provided below.

The variability of size distributions of particles suspended in the studied waters is indirectly indicated by analyses of selected biogeochemical characteristics of fractionated samples, including the relative contributions of particles of individual size fractions to the total mass concentration of particles (SPM) and to the total concentration of chlorophyll a (Chl$a$). An example can be extreme values obtained when considering the contribution of medium and large particles (ML fraction) in these total concentrations. For the ratio $\mathrm{SPM_{ML}}$/SPM ratio the extreme values we recorded were 0.10 and 0.52, and for the Chla_{ML}/Chl$a$ ratio, they were 0 and 0.59.

The collected data also indicate the variability of selected particle composition metrics between the distinguished size fractions. An example can be the average values of the POM/SPM ratio for individual fractions: for the S fraction it was clearly lower and amounted to 0.21, while for the VS and ML fractions the average values were 0.34 and 0.32, respectively.

Based on the results of optical measurements carried out on fractionated samples, it can be concluded that in the case of all analysed optical coefficients, i.e. b_p, a_p, a_d and a_{ph}, on average the S fraction had the largest contribution to their total values, followed by the VS and ML fractions. In the case of the b_p, and also a_d and a_d coefficients, the average contributions of the S fraction in the entire analysed spectral ranges were above 0.6, and in the case of the a_{ph} coefficient (but determined for a limited set of samples only), the average contribution in the entire analysed range was approximately 0.5. However, similarly to the contribution of size fractions to total SPM and Chl$a$ concentrations, we also observed a very large variability in the contribution of size fractions to optical coefficients between individual samples. Referring to examples for selected spectral bands, the S fraction contribution to the $b_p(555)$ coefficient ranged from 0.31 to 0.85, for $a_p(400)$ from 0.37 to 0.81, for $a_d(400)$ from 0.33 to 0.80, and for $a_{ph}(440)$ from 0 to 0.87.

The collected data also allowed the identification of statistical relationships between the SPM_{ML}/SPM ratio, the biogeochemical quantity that indirectly characterises the variability of particle size distributions, and selected characteristics of the optical properties of original (unfiltered) seawater samples. We documented this with examples of best-fit functional relationships obtained by OLS regression. For instance, we observed statistical correlations between the spectral slope of the b_p coefficient, η, and the SPM_{ML}/SPM ratio (see Eq. (3)). However, for η, we also identified the best-fit relationships of this quantity with SPM and POM/SPM, which seem stronger (comparing the values of the coefficient of determination R^2) than the mentioned η vs SPM_{ML}/SPM relationship (see the equations of best-fit function given in Figure 6). We also observed statistical correlations between the SPM-specific coefficient of scattering by particles, $b_p^*(\lambda)$, and SPM_{ML}/SPM (see equations from (4) to (6)). In the case of analyses of the relationship between the SPM-specific coefficient of absorption of either particles or non-algal particles, ($a_p^*(\lambda)$ or $a_d^*(\lambda)$) and SPM_{ML}/SPM, we observed relatively weaker relationships and only in the shortwave part of the analysed spectral range (see Eqs. (8) and (9)).

In our opinion, all the results and statistical relationships documented in this work should be considered when one tries to reach a better understanding of the variability of the optical properties of waters occurring in the Arctic fjords of Spitsbergen. The results obtained here should also be helpful in reaching a more accurate interpretation of the results of various optical measurements, including remote sensing of ocean colour, conducted in this environment. However, due to the qualitative nature of the particle fractionation technique used, it seems advisable to continue research on the relationships between sizes, composition and optical properties of aquatic particles in this complex marine environment.

Acknowledgements

The data collection and preliminary analyses were supported through the National Science Centre, Poland, project no. 2019/35/O/ST10/02874 (project entitled: *Variability of inherent optical properties of seawater in relation to the concentration, composition and size distribution of suspended particulate matter in selected fjords of western Spitsbergen*, awarded to S.B.W.). Partial support for this study, including final analyses and preparation of manuscript for publication, was provided through the Statutory Research Program of the Institute of Oceanology of the Polish Academy of Sciences (IOPAN). We thank our colleagues from IOPAN and the crew of r/v *Oceania* for their assistance in the preparation and execution of fieldwork. We would also like to thank Daniel Koestner and Matthew Kehrli for participating in conducting measurements during one of our cruises.

Authors' contribution

S.B.W. — development of study concept, obtaining main funds to support the study, supervision and participation in preparation of field campaigns, participation in the second field campaign, conducting data analyses, preparation of the original and revised version of the manuscript; D.L. – participation in preparation of field campaigns, implementation of two field campaigns, conducting most laboratory work related to collected samples; J.S.E. – participation in preparation for field campaigns, conducting some laboratory work related to collected samples.

Declaration of competing interest

The authors declare that they have no known competing financial interests or personal relationships that could have appeared to influence the work reported in this paper.

References

Ahn, Y.-H., 1999. *Proprietes optiques des particules biologiques et minerales presentes dans l'ocean. Application: inversion de la reflectance*. PhD thes. Univ. Pierre and Marie Curie, Paris, France.

Babin, M., Morel, A., Fournier-Sicre, V., Fell, F., Stramski, D., 2003. *Light scattering properties of marine particles in coastal and oceanic waters as related to the particle mass concentration*. Limnol. Oceanogr. 48, 843–859. https://doi.org/10.4319/lo.2003.48.2.0843

Babin, M., Stramski, D., 2002. *Light absorption by aquatic particles in the near-infrared spectral region*. Limnol. Oceanogr. 47, 911–915. https://doi.org/10.4319/lo.2002.47.3.0911

Babin, M., Stramski, D., 2004. *Variations in the mass-specific absorption coefficient of mineral particles suspended in water*. Limnol. Oceanogr. 49, 756–767. https://doi.org/10.4319/lo.2004.49.3.0756

Bricaud, A., Morel, A., 1986. *Light attenuation and scattering by phytoplanktonic cells: a theoretical modeling*. Appl. Opt. 25, 571–580.

Ciotti, A.M., Lewis, M.R., Cullen, J.J., 2002. *Assessment of the relationships between dominant cell size in natural phytoplankton communities and the spectral shape of the absorption coefficient*. Limnol. Oceanogr. 47 (2), 404–417.

Davies, E.J., McKee, D., Bowers, D., Graham, G.W., Nimmo-Smith, W.A.M., 2014. *Optically significant particle sizes in seawater*. Appl. Opt. 53, 1067–1074. http://dx.doi.org/10.1364/AO.53.001067

IOCCG Protocol Series, 2018. *Inherent Optical Property Measurements and Protocols: Absorption Coefficient*, [in:] Neeley, A. R. Mannino, A. (Eds.), *IOCCG Ocean Optics and Biogeochemistry Protocols for Satellite Ocean Colour Sensor Validation* Vol. 1.0, IOCCG, Dartmouth,

NS, Canada, 78 pp.
http://dx.doi.org/10.25607/OBP-119

Jonasz, M., Fournier, G.R., 2007. *Light scattering by particles in water. Theoretical and experimental foundations*. Acad. Press, Amsterdam, 704 pp.

Koestner, D., Stramski, D., Reynolds, R.A., 2020. *Assessing the effects of particle size and composition on light scattering through measurements of size-fractionated seawater samples*. Limnol. Oceanogr. 65 (2), 173–190. https://doi.org/10.1002/lno.11259

Meler, J., Litwicka, D., Zabłocka, M., 2023. *Variability of light absorption coefficients by different size fractions of suspensions in the southern Baltic Sea*, Biogeosciences 20, 2525–2551. https://doi.org/10.5194/bg-20-2525-2023

Mobley, C. D. (Ed.), 2022. *The Oceanic Optics Book*, International Ocean Colour Coordinating Group (IOCCG), Dartmouth, NS, Canada, 924 pp. https://doi.org/10.25607/OBP-1710

Morel, A., Bricaud, A., 1986. *Inherent optical properties of algal cells including picoplankton theoretical and experimental results*. Canadian Bull. Fish. Aquat. Sci. 214, 521–560.

Neukermans, G., Loisel, H., Meriaux, X., Astoreca, R., McKee, D., 2012. *In situ variability of mass- specific beam attenuation and backscattering of marine particles with respect to particle size, density, and composition*. Limnol. Oceanogr. 57 (1), 124–144. https://doi.org/10.4319/lo.2011.57.1.0124

Pearlman, S.R., Costa, H.S., Jung, R.A., McKeown, J.J., Pearson, H.E., 1995. *Solids (section 2540)*, [in:] Eaton, A.D., Clesceri, L.S., Greenberg, A.E. (Eds.), *Standard Methods for the Examination of Water and Wastewater*. American Publ. Health Assoc., Washington, D.C., 2-53–2-64.

Peng, F., Effler, S.W., 2007. *Suspended minerogenic particles in a reservoir: Light-scattering features from individual particle analysis*, Limnol. Oceanogr. 52, 204–216.

Ramírez-Pérez, M., Röttgers, R., Torrecilla, E., Piera, J., 2015. *Cost-Effective Hyperspectral Transmissometers for Oceanographic Applications: Performance Analysis*. Sensors 15, 20967–20989. https://doi.org/10.3390/s150920967

Reynolds, R.A., Stramski, D., Neukermans, G., 2016. *Optical backscattering of particles in Arctic seawater and relationships to particle mass concentration, size distribution, and bulk composition*. Limnol. Oceanogr. 61, 1869–1890. https://doi.org/10.1002/lno.10341

Röttgers, R., Gehnke, S., 2012. *Measurement of light absorption by aquatic particles: improvement of the quantitative filter technique by use of an integrating sphere approach*. Appl. Opt. 51, 1336–1351.

Stoń, J., Kosakowska, A., 2002. *Phytoplankton pigments designation – an application of RP-HPLC in qualitative and quantitative analysis*. J. Appl. Phycol. 14, 205–210. https://doi.org/10.1023/A:1019928411436

Stoń-Egiert, J., Kosakowska, A., 2005. *RP-HPLC determination of phytoplankton pigments comparison of calibration results for two columns*. Mar. Biol. 147, 251–260. https://doi.org/10.1007/s00227-004-1551-z

Stoń-Egiert, J., Łotocka, M., Ostrowska, M., Kosakowska, A., 2010. *The influence of biotic factors on phytoplankton pigment composition and resources in Baltic ecosystems: new analytical results*. Oceanologia 52(1), 101–125. https://doi.org/10.5697/oc.52-1.101

Stramski, D., Babin, M., Woźniak, S.B., 2007. *Variations in the optical properties of terrigenous mineral-rich particulate matter suspended in seawater*. Limnol. Oceanogr. 52, 2418–2433. https://doi.org/10.4319/lo.2007.52.6.241

Stramski, D., Kiefer, D.A, 1991. *Light scattering by microorganisms in the open ocean*. Prog. Oceanogr. 28, 343–383. https://doi.org/10.1016/0079-6611(91)90032-H

Stramski, D., Reynolds, R.I., Kaczmarek, S., Uitz, J., Zheng, G., 2015. *Correction of pathlength amplification in the filter-pad technique for measurements of particulate absorption coefficient in the visible spectral region*. Appl. Opt. 54, 6763–6782. https://doi.org/10.1364/AO.54.006763

Stramski, D., Woźniak, S.B., Flatau, P.J., 2004. *Optical properties of Asian mineral dust suspended in seawater*. Limnol. Oceanogr. 49, 749–755. https://doi.org/10.4319/lo.2004.49.3.0749

Tassan, S., Ferrari, G.M., 1995. *An alternative approach to absorption measurements of aquatic particles retained on filters*. Limnol. Oceanogr. 40(8), 1358–1368.

Tassan, S., Ferrari, G.M., 2002. *A sensitivity analysis of the 'transmittance-reflectance' method for measuring light absorption by aquatic particles*. J. Plankton Res. 24(8), 757–774. https://doi.org/10.1093/plankt/24.8.757

Woźniak, B., Dera, J., 2007. *Light Absorption in Sea Water*. Springer, New York.

Woźniak, S.B., Litwicka, D., Stoń-Egiert, J., Stramski, D., 2024. *Variability of inherent optical properties of seawater in relation to the concentration and composition of suspended particulate matter in the coastal Arctic waters of western Spitsbergen*. J. Mar. Syst. 246, 104019. https://doi.org/10.1016/j.jmarsys.2024.104019

Woźniak, S.B., Meler, J., Stoń-Egiert, J., 2022. *Inherent optical properties of suspended particulate matter in the southern Baltic Sea in relation to the concentration, composition and characteristics of the particle size distribution; new forms of multicomponent parameterizations of optical properties*. J. Mar. Syst. 229, 103720. https://doi.org/10.1016/j.jmarsys.2022.103720

Woźniak, S.B., Sagan, S., Zabłocka, M., Stoń-Egiert, J., Borzycka, K., 2018. *Light scattering and backscattering by particles suspended in the Baltic Sea in relation to the*

mass concentration of particles and the proportions of their organic and inorganic fractions. J. Mar. Syst. 182, 79–96.
https://doi.org/10.1016/j.jmarsys.2017.12.005

Woźniak, S.B., Stramski, D., Stramska, M., Reynolds, R.A., Wright, V.M., Miksic, E.Y., Cichocka, M., Cieplak, A.M., 2010. *Optical variability of seawater in relation to particle concentration, composition, and size distribution in the nearshore marine environment at Imperial Beach, California*. J. Geophys. Res. Oceans 115, C08027.
https://doi.org/10.1029/2009JC005554